Estimating Coronary Perfusion Pressure during Cardiopulmonary Resuscitation using Physiological Parameters and Machine Learning

Maryam Valipour

A Thesis

in

The Department

of

Concordia Institute for Information Systems Engineering (CIISE)

Presented in Partial Fulfillment of the Requirements

for the Degree of

Master of Applied Science (Quality Systems Engineering) at

Concordia University

Montréal, Québec, Canada

July 2025

CONCORDIA UNIVERSITY

School of Graduate Studies

This is to certify that the thesis prepared

By: **Maryam Valipour**

Entitled: **Estimating Coronary Perfusion Pressure during Cardiopulmonary Resuscitation using Physiological Parameters and Machine Learning**

and submitted in partial fulfillment of the requirements for the degree of

Master of Applied Science (Quality Systems Engineering)

complies with the regulations of this University and meets the accepted standards with respect to originality and quality.

Signed by the Final Examining Committee:

_____ Chair & Examiner
Dr. Roch Glitho

_____ Examiner
Dr. Manar Amayri

_____ Supervisor
Dr. Jamal Bentahar

_____ Co-supervisor
Dr. Lyes Kadem

Approved by _____
Dr. Chun Wang, Chair
Department of Concordia Institute for Information Systems Engineering (CIISE)

_____ 2025

_____
Mourad Debbabi, Dean
Faculty of Engineering and Computer Science

Abstract

Estimating Coronary Perfusion Pressure during Cardiopulmonary Resuscitation using Physiological Parameters and Machine Learning

Maryam Valipour

Sudden cardiac arrest remains a critical global health issue with survival rates stagnating below 10%. Current resuscitation strategies often employ a "one-size-fits-all" approach, neglecting individual patient variations. Coronary perfusion pressure (CPP), the most reliable indicator of cardiopulmonary resuscitation (CPR) effectiveness, requires invasive catheterization for real-time measurement, limiting its utility in emergency and out-of-hospital scenarios. This study introduces a novel framework for real-time, continuous, non-invasive, and calibration-free CPP estimation, leveraging photoplethysmography (PPG) and electrocardiography (ECG) signals integrated with machine learning. Our method employs an animal-based data-split strategy to enhance generalization and eliminate the need for calibration to new animals, making it highly applicable to real-world situations. A dataset of 13 swine models was collected, each subjected to ventricular fibrillation and resuscitated using mechanical chest compressions aligned with American Heart Association guidelines. During these procedures, solid-state pressure catheters in the aortic arch and right atrium recorded CPP, while PPG and ECG signals were gathered simultaneously. The data was transformed into three different input modalities: single-cycle, rolling-window multi-cycle, and stacked multi-cycle. Among these input modalities, the stacked multi-cycle modality, paired with a transformer model trained using scheduled sampling and utilizing both PPG and ECG signals, achieved the best performance. This configuration yielded a mean absolute error of 6.410 mmHg on an animal-based data split, outperforming previous models. This work highlights the transformative potential of PPG and ECG-based models for non-invasive CPP prediction, enabling personalized

and data-driven CPR adjustments. By providing subject-based, real-time feedback, this approach promises to optimize myocardial blood flow, improve resuscitation outcomes and advance the standard of care in cardiac arrest management.

Acknowledgments

I would like to express my deepest gratitude to my supervisors, Dr. Jamal Bentahar and Dr. Lyes Kadem, for their invaluable guidance, support, and encouragement throughout the course of this thesis. Their expertise and mentorship have been essential in shaping this work and my development as a researcher.

I would also like to sincerely thank the team at IMPACK CPR, especially Dr. Lawrence Leroux and Etienne Fortin, for their collaboration, insightful feedback, and technical support during this thesis. Their contributions were instrumental in this thesis.

I am grateful to my friends and family for their ongoing support. I would especially like to thank my parents for their continuous encouragement, which made it possible for me to carry out this research.

Contents

List of Figures

List of Tables

Chapter 1

Introduction

Chapter 1 provides an overview of the problem addressed and outlines the motivation, key contributions, and organization of the thesis.

1.1 Motivation

Sudden cardiac arrest (SCA) is a leading cause of death globally and demands immediate and effective cardiopulmonary resuscitation (CPR) to restore circulation and preserve life. CPR involves repetitive chest compressions to artificially maintain blood flow, and its quality, specifically compression depth, rate, and consistency directly impacts the likelihood of return of spontaneous circulation (ROSC).

Despite improvements in CPR guidelines, survival rates for out-of-hospital cardiac arrest remain below 10% [1]. A central reason for this stagnation is the lack of individualized feedback during resuscitation. Current CPR protocols rely on generalized targets, such as compressing at least 100 times per minute to a depth of at least 50 mm in adults [1]. However, these uniform recommendations fail to account for subject-specific anatomical and physiological differences that critically impact outcomes.

A key physiological indicator of successful resuscitation is coronary perfusion pressure (CPP), defined as the difference between aortic diastolic and right atrial pressure. CPP reflects the myocardial blood flow generated by chest compressions and is strongly associated with the likelihood

of return of spontaneous circulation (ROSC) [2]. However, CPP is currently typically measured through invasive catheterization, which is impractical and risky in emergency settings, especially during pre-hospital or emergency scenarios.

Recent research has explored the use of non-invasive physiological signals, particularly photoplethysmography (PPG) and electrocardiography (ECG) for estimating blood pressure. These signals can capture important hemodynamic and electrical information from the heart. However, most existing non-invasive approaches focus on estimating general blood pressure metrics such as systolic or diastolic pressure, and are typically developed outside the context of CPR. Only a few studies specifically target CPR scenarios, or predict CPP. Emerging research has shown that PPG and ECG serve as indicators of myocardial perfusion during CPR and may reflect CPP values [3–6]. If leveraged effectively using machine learning (ML), these signals have the potential to offer individualized feedback on perfusion status and inform optimal compression strategies in real time—enhancing CPR effectiveness and improving outcomes.

1.2 Problem Statement

Despite the clinical importance of coronary perfusion pressure (CPP) as a hemodynamic predictor of resuscitation success, there is currently no reliable method for estimating CPP non-invasively, continuously, and calibration-free during cardiopulmonary resuscitation (CPR). Existing techniques rely on invasive monitoring techniques. Though accurate, they are impractical in emergency and out-of-hospital settings due to their complexity, risk, and lack of portability.

Although machine learning (ML) approaches using PPG and ECG signals have been explored for general blood pressure estimation, their application to real-time CPP prediction in the context of CPR remains largely unexplored. Existing models often rely on hand-crafted features and subject-specific calibration, limiting their real-world utility. Moreover, prior studies frequently use random data splits, which overestimate performance and fail to test generalizability across unseen patients, an essential requirement for clinical deployment.

Therefore, there is a critical need for a robust, calibrationfree, and non-invasive framework capable of estimating CPP in real time using raw physiological signals during CPR. Such a system

should eliminate the need for manual feature engineering, avoid subject-specific fine-tuning, generalize effectively across individuals, and operate without relying on invasive procedures. Additionally, it should support dynamic, data-driven feedback to guide and personalize CPR delivery. This thesis aims to address these challenges through the development and evaluation of an ML-based pipeline for real-time CPP prediction using raw PPG and ECG signals.

1.3 Contributions

This work introduces a novel framework for real-time, continuous, non-invasive, and calibration-free estimation of CPP during CPR. By integrating photoplethysmogram (PPG) and electrocardiogram (ECG) signals with advanced ML models, the proposed approach enables individualized, data-driven adjustments to CPR techniques. Ultimately, this personalized strategy seeks to enhance myocardial blood flow and resuscitation outcomes during cardiac arrest. The key contributions of this paper are:

(1) **Non-invasive and calibration-free CPP estimation:** We propose a non-invasive and calibration-free framework that processes raw PPG and ECG signals to continuously estimate CPP during CPR. By employing a animal-based data-split strategy and tailoring the model to individual animal dynamics, our approach ensures accurate CPP estimation without requiring additional calibration, making it adaptable to real-time clinical scenarios.

(2) **Scheduled sampling for better generalization and temporal robustness:** Scheduled sampling is incorporated as a training strategy to improve the model's ability to capture the temporal dynamics of chest compressions during CPR. By gradually transitioning from ground-truth inputs to model-predicted inputs during training, this method enhances generalization to unseen subjects without requiring calibration, making the model more reliable in real-world CPR applications.

(3) **Novel input modalities:** We consider three different input modalities—including single-cycle, rolling-window multi-cycle, and stacked multi-cycle inputs—to effectively leverage both spectral and temporal features of PPG and ECG signals, enhancing predictive performance and

robustness.

(4) **Comprehensive model evaluation:** We implement and compare a range of classical ML, DL architectures, and models designed specifically for time-series data such as support vector regression, random forests, BiGRUs, Seq2Seq, and Transformers to thoroughly evaluate the effectiveness of the proposed solution in realistic CPR scenarios.

Together, these contributions support the development of a practical, real-time system for personalized resuscitation. By offering rescuers real-time, actionable feedback on animal-based physiological indicators, our system has the potential to elevate CPR from a generalized procedure into an adaptive, data-driven intervention that improves survival outcomes.

1.4 Organization

This thesis is organized as follows. Chapter 2 provides background information on SCA and CPR and a literature review on blood pressure estimation methods, including traditional methods and ML-based approaches. It also highlights existing research gaps specifically in CPR-specific contexts. Chapter 3 describes the experimental setup, including data collection, data preprocessing, the design of the end-to-end ML pipeline, and detailed architecturs of the models used. Chapter 4 presents the results obtained from the three proposed input modalities, followed by a discussion of the model performances. Finally, Chapter 5 summarizes the main findings and discusses future research directions.

Chapter 2

Background and Literature Review

This chapter presents an overview of the physiological and clinical background of sudden cardiac arrest and cardiopulmonary resuscitation. It also reviews existing methods for blood pressure estimation, examines the literature and highlights the gaps in real-time, non-invasive monitoring during resuscitation.

2.1 Sudden Cardiac Arrest

Sudden cardiac arrest (SCA) is a life-threatening condition characterized by an abrupt loss of heart function, resulting in a critical reduction in blood flow to vital organs. This leads to immediate collapse, unconsciousness, and the absence of breathing. Onset is dramatic and without warning, though some may experience preceding chest pain, shortness of breath, palpitations, or dizziness. The most common underlying cause is ventricular fibrillation, a chaotic heart rhythm where the lower chambers (ventricles) quiver instead of pumping blood effectively. This can be triggered by coronary artery disease, heart attacks, cardiomyopathy, inherited conditions, electrolyte imbalances, or in some cases, significant blood loss, trauma, drug overdose, or certain medications.

2.2 Cardiopulmonary Resuscitation

Cardiopulmonary Resuscitation (CPR) is a lifesaving emergency procedure performed when the heart stops beating [7]. Immediate intervention through CPR is crucial to sustain life, as it

temporarily restores blood circulation to the brain and lungs while delivering oxygen until advanced medical care becomes available [1]. It involves chest compressions, which manually pump blood to vital organs like the brain and lungs, and may include rescue breaths (mouth-to-mouth or with a mask) to deliver oxygen to the lungs. The goal of CPR, whether performed manually or with a device, is to maintain blood circulation and oxygenation until circulation and breathing can be restored. If available, a defibrillator (AED) should be used to deliver an electric shock and restore normal heart rhythm. This combination of early CPR and defibrillation improves survival rates in sudden cardiac arrest cases.

Despite its importance, CPR remains inherently inefficient, providing only 10–30% of normal blood flow to the heart and 30–40% to the brain, even when performed according to established guidelines [8–10]. Consequently, survival rates for out-of-hospital cardiac arrest (OHCA) cases remain alarmingly low, typically below 10%, with minimal improvement over the past four decades. In North America alone, approximately 400,000 OHCA cases occur annually [11,12]. A systematic review spanning 1976-2019 reveals a mere global increase of 1.3% increase in survival rates from 8.6% to 9.9%, highlighting the urgent need for continued advancements in resuscitation techniques [13]. These statistics underscore the urgent need for innovations in resuscitation science.

The persistently low survival rates can be attributed to several factors, including the time-sensitive nature of CPR and the quality with which it is performed. For every minute without effective intervention, survival chances decrease by 7–10% [14], and death can occur within minutes if left untreated. Although timely CPR is crucial, its effectiveness also depends on how well compressions are administered. Maintaining consistent compression rate and depth is physically demanding and prone to human error. While alternative approaches like dual-rescuer CPR and mechanical devices like the LUCAS chest compression system aim to address these issues, overall survival rates still remain low [15].

The suboptimal outcomes of CPR are partly due to the complexities of the underlying mechanisms and physiological principles, which are not fully understood. Unfortunately, traditional ”one-size-fits-all” CPR methods disregard critical physiological differences such as chest anatomy, pre-existing conditions, and demographic factors like age, gender, and weight. For instance, guidelines often recommend compressing the lower half of the sternum at the inter-nipple line, assuming

the heart's placement is uniform across all patients. However, Shin [16] found that the left ventricle was located at this landmark in only 20% of individuals. These limitations collectively undermine the effectiveness of CPR and highlight the need for more personalized methods. Personalization of CPR has emerged as a promising strategy to overcome these challenges. By customizing chest compressions to an individual's unique physiological profile, clinicians can better optimize blood flow to the heart and brain.

Coronary perfusion pressure (CPP)—the difference between aortic diastolic pressure and central venous pressure during the relaxation phase of chest compressions—serves as the primary driver of myocardial blood flow [2] and is a key predictor of return of spontaneous circulation (ROSC) [17]. Studies have shown that maintaining a CPP above 20 mmHg significantly increases the likelihood of ROSC [1]. To provide effective feedback to rescuers during CPR, real-time estimation of coronary perfusion pressure (CPP) is essential, as it is a primary determinant of myocardial blood flow during CPR [2]. Accurate CPP estimation can guide adjustments to the rescuer's actions, including the depth, rate, and location of chest compressions, thereby enhancing perfusion and improving patient outcomes.

Real-time CPP monitoring currently relies on invasive catheter-based techniques, limiting its feasibility in both emergency and routine clinical settings. In contrast, non-invasive methods avoid catheterization and estimate blood pressure either intermittently or continuously. Continuous non-invasive techniques use external sensors—such as photoplethysmography (PPG) or electrocardiography (ECG)—to monitor physiological parameters without penetrating the skin or blood vessels. Despite its critical role in medicine and its direct impact on resuscitation success, most non-invasive research to date has focused on non-CPR contexts, primarily estimating general blood pressure metrics such as systolic, diastolic, and mean arterial pressures, leaving a critical gap in resuscitation monitoring strategies.

2.2.1 Blood Pressure Measurement

Blood pressure (BP) is a critical physiological parameter and a key indicator of cardiovascular health. Accurate measurement of BP is essential in both routine clinical care and high-acuity settings such as intensive care units or during cardiopulmonary resuscitation (CPR). Blood pressure

estimation techniques can be broadly categorized into invasive and non-invasive methods, each with specific benefits and limitations.

Invasive approaches involve the insertion of catheters into arteries, typically the radial or femoral, to obtain direct and continuous pressure measurements [18]. These methods are commonly used in intensive care units and during high-risk surgeries where precision is crucial. However, while highly accurate and continuous, invasive monitoring presents significant risks such as infection, bleeding, and vascular damage [19]. Crucially, in time-sensitive situations such as cardiopulmonary resuscitation (CPR), the urgency of intervention and the need to minimize procedural complexity render invasive hemodynamic monitoring impractical. The requirement for rapid action during resuscitation precludes the placement of intravascular catheters, limiting the use of traditional invasive techniques [20].

On the other hand, non-invasive blood pressure measurement methods eliminate many risks associated with invasive techniques. These techniques rely on external sensors and devices to estimate blood pressure without direct vascular access. While they may not achieve the same level of precision as invasive methods, their ease of use and safety profile make them invaluable tools for routine blood pressure assessment and real-time monitoring during emergencies. Within non-invasive methods, there is a distinction between cuff-based and cuffless techniques. Cuff-based methods, like the widely used oscillometric technique, rely on an inflatable cuff to stop and release blood flow. While effective for periodic measurement, these systems are unsuitable for continuous monitoring and interrupt chest compressions during CPR.

Cuffless methods overcome these limitations by enabling continuous, real-time monitoring through unobtrusive sensors. These approaches often rely on physiological signals such as photoplethysmography (PPG) and electrocardiography (ECG). Together, these signals provide valuable information about cardiovascular dynamics and are increasingly used in research to estimate various blood pressure indices without disrupting clinical workflows.

2.3 Literature Review

2.3.1 General Overview

Accurate and continuous blood pressure (BP) monitoring is essential in many clinical settings, particularly during time-sensitive interventions such as cardiopulmonary resuscitation (CPR). Traditional BP measurement methods, such as cuff-based sphygmomanometers and intra-arterial lines, are either intermittent or invasive, limiting their applicability in dynamic, real-time environments. As a result, there has been increasing interest in non-invasive, cuffless approaches capable of providing continuous physiological feedback.

Among these, methods that leverage photoplethysmography (PPG) and electrocardiography (ECG) signals have gained widespread attention. PPG captures blood volume changes in the microvascular bed by measuring variations in transmitted or reflected light, offering an indirect but reliable indicator of tissue perfusion [20]. ECG, on the other hand, records the heart's electrical activity and provides precise information on cardiac timing. These signals are often used to utilize known relationships between cardiovascular dynamics and blood pressure to infer hemodynamic states. They are used to extract time-based or frequency-based features that correlate with arterial stiffness, vascular resistance, or pulse propagation, which in turn are related to blood pressure.

Several traditional techniques have been proposed based on these physiological relationships, including Pulse Transit Time (PTT), Pulse Arrival Time (PAT), Pulse Wave Velocity (PWV), and Heart Rate Variability (HRV). These methods are attractive due to their simplicity and physiological interpretability. However, they also face key limitations: they typically require individual calibration, are sensitive to signal noise and artifacts, and often fail to generalize across different populations or physiological conditions.

To address these limitations, machine learning (ML) models have emerged as a powerful alternative. Unlike traditional methods that rely on hand-crafted features and linear assumptions, ML models have the potential to process raw waveform data directly, learning complex, nonlinear mappings between input signals and target outputs. When properly trained and validated, ML models have the potential to generalize across subjects without the need for calibration, making them especially promising for real-time, non-invasive blood pressure estimation during CPR and other

high-stakes scenarios.

However, while numerous studies have applied ML models for BP estimation in non-CPR contexts, relatively few have explored their application during CPR or for the estimation of coronary perfusion pressure (CPP). This is a significant gap, considering that CPP is the most reliable hemodynamic predictor of return of spontaneous circulation (ROSC) and a critical target during resuscitation efforts. Several studies have demonstrated physiological correlations between PPG and ECG features and CPP or perfusion quality [3–6]. For example, PPG waveforms can can help determine the quality of chest compressions in patients without spontaneous circulation due to its pulsatile nature; optimal compression depth and rate typically yield more pronounced signals, indicating effective perfusion [3]. Features extracted from ECG waveforms such as the amplitude spectrum area shows correlations with CPP during compressions [4,5], and real-time ECG waveforms also appear responsive to reperfusion events, providing immediate insight for guiding resuscitation [6].

To set the stage for CPP estimation during CPR, the following subsection reviews machine learning methods for non-invasive BP estimation in both non-CPR and CPR contexts. The literature is organized into two main categories: (1) models based on manual feature extraction from PPG and ECG signals, and (2) models that operate directly on raw waveform inputs. These studies form the methodological foundation upon which CPR- and CPP-specific approaches can be built. A subsequent section will then focus on the limited but growing body of work that explores ML-based CPP prediction and physiologically guided feedback in CPR settings.

2.3.2 Machine Learning Methods

As a result, there is increasing interest in continuous, non-invasive techniques that integrate signals such as PPG and ECG with ML to estimate blood pressure and other hemodynamic parameters in real time. Within these non-invasive, machine learning integrated methodologies, two main modeling paradigms have emerged for predicting blood pressure: models that utilize manually extracted features from physiological signals and models that work directly on raw waveforms.

Manual Feature Extraction

A number of studies have proposed blood pressure estimation frameworks that rely on handcrafted features extracted from photoplethysmography (PPG) and electrocardiography (ECG) signals. These features, typically frequency domain, time domain, or morphological characteristics such as the height and width of the waveform at various key points, are then used as inputs to machine learning models [21–35].

A representative example is provided by Mejía-Mejía et al. [26] who extracted a broad set of features from these signals derived from pulse rate variability. These included time-based metrics (such as the mean and variability of inter-beat intervals), frequency-based components (including low- and high-frequency power and their ratios), and a wide range of nonlinear features. Nonlinear metrics encompassed characteristics from Poincaré plots, entropy measures, fractal dimensions, and signal complexity—all of which were used to classify patients into hypertensive, normotensive, and hypotensive categories. This example illustrates the diversity and richness of features that can be engineered manually to support blood pressure classification or regression models.

Classical algorithms such as logistic regression, support vector regression (SVR), k-nearest neighbors (k-NN), random forests (RF), and gradient boosting have commonly been applied in these studies. Suzuki et al. [21] applied the Taguchi method to identify signal-to-noise ratio–based features that are robust to noise and subject variability when used in regression models. Shen et al. [22] combined features from PPG and ECG signals and used stepwise regression for blood pressure estimation. Kachuee et al. [23] extracted multiple physiological parameters from PPG waveforms and applied regression models including Support Vector Regression (SVR). Miao et al. [24] used multivariate regression and SVR models on features selected via roulette wheel selection from ECG and PPG signals. Zhang et al. [25] used a classification and regression tree (CART) model, identifying pulse transit time (PTT) and heart rate as key features. Mejía-Mejía et al. [26] applied handcrafted time, frequency, and nonlinear features extracted from pulse rate variability (PRV) derived from PPG signals to k-Nearest Neighbors (k-NN), and support vector machines (SVMs) algorithms to classify hypertensive, normotensive, and hypotensive states in critically ill patients, achieving promising results in both classification and regression tasks.

Some studies applied deep learning architectures to these hand-crafted features. Xing et al. [27] used fast Fourier transform (FFT)-based features from PPG signals with a feedforward artificial neural network (ANN). Wang et al. [28] employed the multi-taper method (MTM) to derive features such as diastolic time and systolic upstroke time along with spectral features at lower frequencies from PPG waveforms, which were fed into an ANN trained on MIMIC data. Roy et al. [29] extracted features from the PPG waveform and used them as input to a novel proposed Temporal Convolutional Network (TCN).

To better model temporal dependencies, several studies incorporated time-series–oriented architectures. Senturk et al. [30] fed 22 time-domain features from ECG and PPG into a bidirectional long short-term memory loss (LSTM). Su et al. [31] improved LSTM performance by incorporating residual connections. Mejia et al. El-Haji et al. [32] extracted 52 features from the PPG signal and its derivatives and used them as input to a BiLSTM model enhanced with an attention mechanism. Ma et al. [33] leveraged a Transformer-based model applied to features extracted from PPG signals in both the time and frequency domains.

Hybrid frameworks that combine different neural network architectures and methods have also been investigated to capture the temporal and spectral nature of physiological signals more effectively. Another study by Senturk et al. [34] presented a novel hybrid model that integrates principal component analysis (PCA) with long short-term memory (LSTM) networks based on PPG signals. The study proposes a hybrid model that extracts 12 time-domain features and applies PCA to obtain 10 new features from the PPG signals. These features are then combined and used to predict blood pressure values using the LSTM-NN model. Kumer et al. [35] developed a hybrid deep learning framework called CS-NET that combines CNNs with SVM for blood pressure classification using PPG signals. The model leverages super-resolution spectrograms generated from PPG signals as input features.

Raw-Signal-based Approaches

In contrast to feature-engineered methods, several studies have leveraged raw PPG or ECG waveforms directly as inputs to machine learning models. This approach enables data-driven algorithms to learn salient patterns automatically without the need for handcrafted features. In [36],

Table 2.1: Literature on manual feature extraction methods for blood pressure estimation

Model Category	Study	Model Used
Classical ML		
	Suzuki et al. (2013) [21]	Regression Model
	Shen et al. (2015) [22]	Stepwise Regression Model
	Kachuee et al. (2015) [23]	Regression Model, SVR
	Miao et al. (2017) [24]	Multivariate Regression Model, SVR
	Zhang et al. (2018) [25]	CART Model
	Mejia et al. (2021) [26]	k-NN, SVR
Deep Learning Models		
	Xing et al. (2016) [27]	ANN
	Wang et al. (2018) [28]	ANN
	Roy et al. (2022) [29]	Temporal Convolutional Network (TCN)
Time-Series–Oriented Models		
	Senturk et al. (2018) [30]	BiLSTM
	Su et al. (2018) [31]	Residual LSTM
	El-haji et al. (2021) [32]	BiLSTM+attention
	Ma et al. (2022) [33]	Transformer Model
Hybrid Models		
	Senturk et al. (2020) [34]	LSTM-NN
	Kumar et al. (2023) [35]	CS-NET (CNN + SVM)

the performance of convolutional neural networks (CNNs) applied to raw physiological signals was compared with conventional manual feature extraction methods. The study found that models trained on raw signals outperformed those using handcrafted features, demonstrating improved accuracy and computational efficiency.

Classical machine learning models have also been applied in this context. For instance, Mousavi et al. [37] applied classical machine learning algorithms, including decision tree regression (DTR), support vector regression (SVR), adaptive boosting regression, and random forest regression models directly to raw PPG signals, with random forests yielding the best performance.

Other studies utilized deep learning architectures such as multilayer perceptrons (MLPs) and convolutional neural networks (CNNs) to extract spatial and morphological features from raw signals. Schlesinger et al. [38] proposed a novel calibration-based approach for blood pressure estimation using Siamese neural networks. This architecture employed two identical subnetworks applied to filtered PPG signals from the MIMIC II database, with spectro-temporal features extracted via CNNs. Vardhan et al. [39] introduced BP-Net, a U-Net–based deep learning model that performs signal-to-signal translation from PPG to arterial blood pressure (ABP) waveforms, eliminating the need for handcrafted features altogether.

To better exploit temporal information in raw signals, time-series models such as recurrent neural networks (RNNs) and attention mechanisms have also been adopted. In one such study, Sideris et al. [40] used RNNs to estimate ABP from PPG signals obtained from finger pulse oximeters, demonstrating the model's ability to capture long-term temporal dependencies.

Furthermore, hybrid deep learning frameworks that integrate MLPs, CNNs, and RNNs have been proposed to capture both spatial and temporal dynamics. Slapničar et al. [41] presented a residual spectro-temporal deep neural network that processes raw PPG signals and their derivatives, combining both temporal and frequency-domain information. Esmaelpoor et al. [42] introduced a two-stage model that first applies CNNs to extract local morphological features from PPG signals, followed by LSTM layers to capture temporal dependencies. Similarly, Baker et al. [43] proposed a CNN–LSTM hybrid model that processes raw ECG and PPG waveforms to estimate systolic, diastolic, and mean arterial pressure continuously and without reliance on handcrafted features such as PTT.

CPR Settings and Limitations

As previouly mentioned, both PPG and ECG provide continuous, real-time data about a patient's cardiovascular status. When integrated with machine learning (ML), these waveforms could potentially be used to estimate coronary perfusion pressure (CPP) in real-time. This could enable the optimization of CPR parameters—such as compression depth, rate, and hand placement—based on the estimated CPP. By providing real-time feedback on the cardiovascular response of patients,

Table 2.2: Literature on raw signal input methods for blood pressure estimation

Model Category	Study	Model Used
Classical ML		
	Mousavi et al. (2019) [37]	DT, SVR, Adaptive Boosting, RF
Deep Learning Models		
	Schlesinger et al. (2020) [38]	Siamese CNNs
	Vardhan et al. (2021) [39]	U-Net
Time-Series–Oriented Models		
	Sideris et al. (2016) [40]	RNN
Hybrid Models		
	Slapničar et al. (2019) [41]	Residual Spectro-Temporal DNN
	Esmaelpoor et al. (2020) [42]	Two-Stage CNN + LSTM
	Baker et al. (2021) [43]	CNN–LSTM

this approach empowers rescuers to adapt their CPR technique on the scene, optimizing compression depth, rate, and rhythm to maximize blood flow and CPP. By focusing on improving CPP, the most reliable physiological predictor of ROSC, this approach has the potential to enhance blood flow and improve survival rates.

Despite progress in non-invasive ML-based blood pressure estimation, few studies target emergency scenarios such as CPR, where continuous and calibration-free estimates of blood pressure and specifically CPP are critical. Among the limited investigations in this domain, Gandhi et al. [44] presented a machine learning framework for predicting CPP in a porcine CPR model, relying on invasive aortic and right atrial pressure measurements. While their findings demonstrated the potential of ML for CPP prediction, the dependence on historical invasive CPP data limits clinical applicability. Park et al. [45] proposed a non-invasive approach using a single earlobe PPG sensor and an LSTM model to estimate systolic and diastolic blood pressure during CPR, illustrating the potential of real-time feedback without the need for arterial catheters. More recently, Jiang et al. [46] investigated a non-invasive method for CPP estimation in a porcine CPR model, utilizing manually

extracted ECG and PPG features in a random forest framework. Their results further highlight the promise of ML-based approaches for improving CPR outcomes while avoiding invasive procedures.

Table 2.3: Literature review on studies focused in CPR settings

Setting	Input Type	Study	Output Estimated	Approach
Invasive Estimation				
	Historical invasive CPP	Gandhi et al. (2018) [44]	CPP	ML framework using invasive aortic and right atrial pressures (porcine CPR model)
Non-Invasive Estimation				
	Manual Feature Extraction	Jiang et al. (2024) [46]	CPP	Random Forest on manually extracted ECG + PPG features (porcine CPR model) using random-split
	Raw Signal Input	Park et al. (2020) [45]	SBP, DBP	LSTM on raw PPG signals from earlobe sensor to estimate SBP and DBP during CPR

Many existing approaches, including those outside of CPR applications, frequently rely on a random split (commonly 80% for training and 20% for testing) for model evaluation. In such splits, recordings from the same subject may appear in both the training and testing sets. Although straightforward, this method can be problematic in real-world clinical scenarios where models must be applied to entirely new subjects whose physiological signals may differ substantially due to variations in health status, demographics, and other factors [41]. Consequently, random splitting often fails to capture these subject-specific differences, potentially overestimating a model's true performance in practice.

To address this limitation, a subject-based split is employed. In this approach, all data from specific subjects is excluded from training and used exclusively for testing, thus more realistically simulating real-world deployment. However, subject-based splits tend to produce higher errors [41, 47] and often yield model performances that do not meet Association for the Advancement of Medical Instrumentation (AAMI) standards. Some researchers have attempted to overcome these

challenges through personalization, wherein a model is fine-tuned using a small amount of data from the target subject [41, 48, 49]. While personalization can significantly improve results, it typically requires invasive calibration and is therefore impractical in urgent CPR scenarios.

Given these limitations, there is a critical need for continuous, calibration-free systems capable of providing reliable CPP estimates in real time, especially in high-stakes CPR settings. To address this gap, this thesis proposes a robust, non-invasive ML-based framework for continuous, calibration-free CPP estimation, eliminating the necessity for subject-specific calibration and prioritizing generalizability. This approach aims to guide real-time, life-saving interventions in critical care environments.

Chapter 3

Methodology

To estimate CPP during CPR, we employed a systematic pipeline encompassing data collection, preprocessing, segmentation, feature extraction, and model evaluation. The process begins with the collection of physiological signals, including aortic pressure, central venous pressure (CVP), photoplethysmography (PPG), and electrocardiogram (ECG) signals. The recorded data are subjected to signal quality assessment, noise filtering, and segmentation into compression–decompression cycles (CDCs). For each CDC, the PPG and ECG waveforms and target CPP values are determined and transformed into distinct input modalities, including single-cycle, rolling-window multi-cycle, and stacked multi-cycle formats. In the training phase, the data are split into training and testing sets, normalized, and processed using various ML and DL models. Finally, the performance of the models are evaluated using metrics such as Mean Absolute Error (MAE), standard deviation error (SDE), and Pearson Correlation Coefficient (r-value).

Figure 3.1 illustrates the entire workflow, providing a high-level overview of the methodology used in this study. Each component of the workflow is detailed in the subsections below, providing an in-depth explanation of the methodology and rationale behind each step.

3.1 Experimental Data

In this study, we performed experiments on 13 adult pigs (35–40 kg) by inducing ventricular fibrillation (VF) cardiac arrest through electrical impulses delivered via transcutaneous electrical

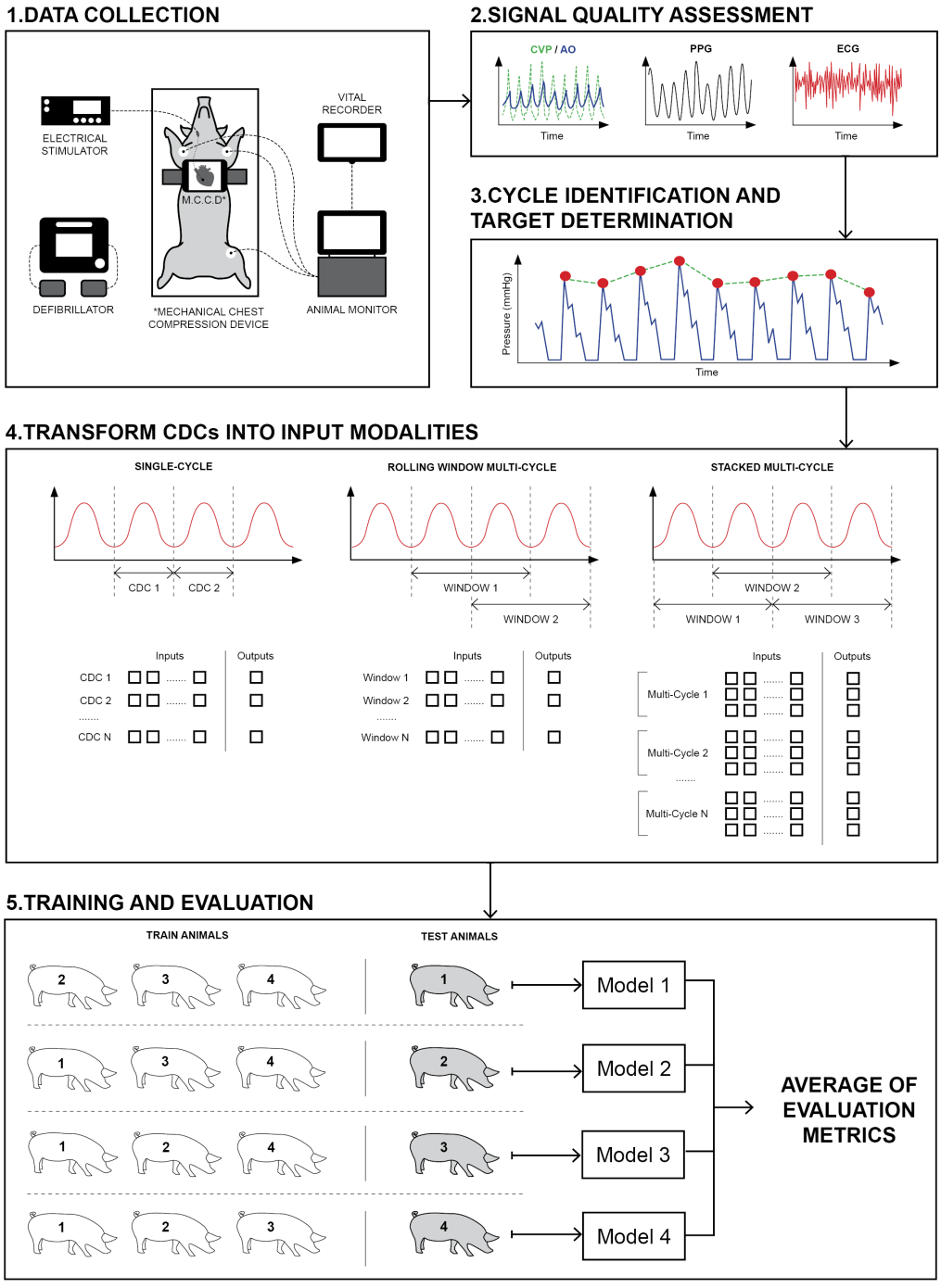

Figure 3.1: Pipeline for coronary perfusion pressure (CPP) estimation during cardiopulmonary resuscitation (CPR), including the stages of data collection, signal quality assessment, transformation of CDCs into input modalities, and model training and evaluation.

induction (TCEI). The pigs were subsequently resuscitated using mechanical chest compressions in accordance with the American Heart Association (AHA) guidelines.

All animals were premedicated with intramuscular ketamine (7 mg/kg), midazolam (0.5 mg/kg), and atropine (0.04 mg/kg). Anesthesia was maintained with inhaled isoflurane (1–2%). Anesthesia levels were monitored to ensure no pain or distress occurred throughout the experiment. Each pig was intubated with a 7.0 mm endotracheal tube and mechanically ventilated with a tidal volume of 10 mL/kg. The respiratory rate was adjusted to maintain an end-tidal CO_2 ($ETCO_2$) between 30–40 mmHg, with a positive end-expiratory pressure (PEEP) of 5 cm H_2O. The fraction of inspired oxygen (FiO_2) was initially set at 100% during preparation and then reduced to 21% five minutes before VF induction.

CPP was continuously measured using solid-state pressure catheters placed in the aortic arch and right atrium, enabling simultaneous recordings of aortic pressure (Ao) and central venous pressure (CVP). In addition to these pressure measurements, photoplethysmography (PPG) signals were captured at the earlobe, and electrocardiogram (ECG) signals were recorded from lead I. The ECG and PPG signals were sampled at 500 Hz, while Ao and CVP signals were sampled at 125 Hz. Additional monitoring included continuous measurement of pulse oximetry, capnography ($ETCO_2$), and invasive pressures using an Intellivue MP70 monitor (Philips), with all data recorded through VitalRecorder software (VitalDB).

Experimentation have taken place at Montreal Heart Institute, a CCAC (Canadian Council on Animal Care) accredited laboratory. This study was carried out according to the applicable ARRIVE guidelines. Animals were treated in accordance with the recommendations of the guidelines on the Care and Use of Laboratory Animals issued by the Canadian Council on Animals and approved by the Institutional Animal Care and Use Committee (Project #2023-3224). A certified and licensed veterinarian supervised the studies to make sure they were done in compliance with Health Canada and CCAC guidelines.

3.2 Signal Quality Assessment

PPG and ECG signals, though essential for physiological monitoring, are prone to various types of noise. PPG waveforms can be disrupted by motion artifacts, baseline drift, and inadequate peripheral perfusion [50], while ECG signals can exhibit baseline wandering, powerline interference, muscle artifacts, and other noise sources [51]. We first evaluated the overall quality of each pig's recording during cardiac arrest, and any recording showing flat lines or peaks caused by sensor interruptions or electrode disconnections for the majority of time was excluded from further analysis. For the remaining signals, effective noise reduction was critical for reliable data analysis. A fourth-order Butterworth low-pass filter with a 5 Hz cutoff was applied to PPG signals, followed by additional cleaning using the method by [52] (implemented in the NeuroKit2 package in Python). For ECG, baseline wandering was removed by a median filter, after which a fourth-order Butterworth band-pass filter between 3 and 30 Hz was used to eliminate remaining noise. These steps ensured that subsequent analyses were based on cleaner, higher-quality signals.

3.3 Cycle Identification and Target Determination

Following noise reduction, the data were segmented into compressiondecompression cycles (CDCs). During cardiac arrest, CPP is calculated as the diastolic blood pressure minus the CVP in the decompression (relaxation) phase of chest compressions [1]. To determine the maximum CPP within each CDC, we segmented the Ao and CVP waveforms into individual cycles. We then computed CPP by subtracting CVP from Ao and identified its maximum value during the decompression phase of each cycle. Figure 3.2 illustrates this procedure.

This value served as the target CPP estimate for the corresponding compression–decompression cycle (CDC). Since the likelihood of recovery during CPR is closely linked to maintaining circulation and a sufficient CPP, we restricted our data to CDCs where CPP ranged from 10 to 50 mmHg. This threshold range was chosen because CPP values above 50 mmHg are commonly associated with patient survival. Any beats with CPP outside the 10–50 mmHg interval, along with their associated PPG and ECG data, were removed.

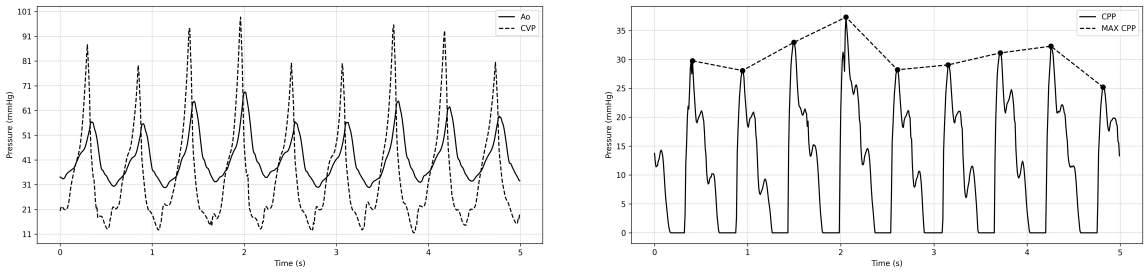

(a) (b)

Figure 3.2: Identification of the maximum coronary perfusion pressure (CPP) during the decompression phase of chest compressions. (a) aortic and central venous pressure, and (b) coronary perfusion pressure (CPP) along with its maximum value during CDCs.

3.4 Transform CDCs into Input Modalities

After segmenting the data into compression–decompression cycles (CDCs), we propose three different input modalities for ML models. Each modality incorporates PPG and ECG signals in a specific way to capture various degrees of temporal and spectral information.

3.4.1 Single-Cycle Input Modality

In the first modality, we treat each compression–decompression cycle independently. The PPG and ECG waveforms from a single cycle constitute the input, while the maximum CPP in that cycle is the output. Both signals are resampled to a uniform length (50 samples each) for straightforward analysis and model training. This approach does not preserve the temporal aspect across cycles.

We evaluate a range of classical ML models, including support vector regression, random forest, k-nearest neighbors, and gradient-boosted regression trees, as well as DL architectures such as fully connected multi-layer perceptrons (MLPs) and convolutional neural networks (CNNs). In each case, we compare the performance of models trained on only PPG signals, only ECG signals, or both signals together. In the case of using PPG and ECG waveforms together, the two signals are concatenated horizontally, forming a 1D array of 100 elements.

3.4.2 Rolling-Window Multi-Cycle Input Modality

The second modality incorporates temporal dependencies by using a rolling window of several consecutive cycles as input. As mentioned, each cycle of PPG and ECG is originally 50 samples in length, capturing one complete compression–decompression cycle (CDC). We concatenate the waveforms from the selected window size horizontally and then resample the concatenated signal back to 50 samples to ensure a uniform input size for further analysis. This resampled signal forms a single input sample for models.

Next, the window shifts by one cycle, creating overlapping segments. For each window, the target CPP is computed as the average of the maximum CPP values from all cycles in that window. This approach retains some temporal information over multiple cycles. The same classical and DL methods used in the first modality are applied here. As in the single-cycle approach, we test both classical ML and DL models with either PPG alone, ECG alone, or both signals concatenated horizontally.

3.4.3 Stacked Multi-Cycle Input Modality

The third modality also uses multiple consecutive cycles but stacks them vertically instead of horizontally. Specifically, for a chosen window size, each cycle's PPG and ECG waveforms are arranged one on top of the other, creating a 2D array of dimensions $[(\text{window size} \times 50)]$. Again, the window shifts by one cycle to create overlapping samples. Unlike the second modality, the target CPP for this arrangement is defined as the maximum CPP in the next cycle. This approach is more amenable to advanced sequence-based models such as bidirectional GRU networks, sequence-to-sequence architectures (with and without attention), Transformer models, and hybrid bidirectional GRU–CNN layers. These models are trained on PPG alone, ECG alone, or both signals together. When combining PPG and ECG, each window slice can be stacked horizontally, resulting in a 1D array of length 100 per cycle, then stacked vertically across cycles, resulting in a 2D array of $(\text{window size} \times 100)$.

3.5 Training Pipeline

3.5.1 Animal-based Splitting

In both CPR and non-CPR settings, previous endeavours often rely on subject-specific calibration or personalization, limiting their feasibility for rapid, real-time deployment in emergency situations such as CPR. Furthermore, many machine learning (ML) models in prior work are evaluated using random data splits, allowing recordings from the same individual to appear in both training and testing sets. This setup can significantly inflate performance metrics and fails to reflect true generalization to unseen patients, which is a requirement for real-world deployment. In contrast, subject-based data splits, where test subjects are excluded entirely from training, offer a more realistic evaluation of a model's robustness but are rarely adopted due to the low performance of the models in that scenario.

Thus, after transforming the data into the chosen input modality, it is divided into training and testing sets. In this study, we employ a subject-based split using the leave-one-subject-out (LOSO) cross-validation approach. In LOSO, data from a single subject is designated as the test set, while data from all remaining subjects are used for training. The model is trained on the training subjects and then evaluated on the test subject. This process is repeated iteratively until every subject has been used as the test set exactly once. The performance metrics are averaged across all subjects to provide the overall results. By ensuring that no data from a test subject is included in the training set, the LOSO evaluation robustly assesses the model's capability to generalize to unseen subjects, simulating real-world scenarios where models must perform on entirely new individuals.

3.5.2 Data Normalization

After constructing the input modalities, we apply min–max normalization across the combined dataset by identifying its global minimum and maximum values. All PPG and ECG waveforms of length 50 are then rescaled to the [0, 1] range to ensure consistency across different subjects and recordings. The normalization is expressed as follows:

$$PPG_{\text{scaled}} = \frac{PPG - \min_{\text{global}}(\mathcal{PPG})}{\max_{\text{global}}(\mathcal{PPG}) - \min_{\text{global}}(\mathcal{PPG})} \tag{1}$$

$$ECG_{\text{scaled}} = \frac{ECG - \min_{\text{global}}(\mathcal{ECG})}{\max_{\text{global}}(\mathcal{ECG}) - \min_{\text{global}}(\mathcal{ECG})}, \tag{2}$$

where $\min_{\text{global}}(\mathcal{PPG})$ and $\max_{\text{global}}(\mathcal{PPG})$ denote the global minimum and maximum values, respectively, computed over all PPG signals. The same applies for ECG. This global normalization ensures that signals from different subjects and recording sessions are comparable within a unified scale.

3.5.3 Scheduled Sampling

In the third input modality (stacked multi-cycle), time-series models often require the previous target values to predict the next one. However, during CPR, invasive CPP measurements from past time steps are unavailable. To address this, we employ scheduled sampling [53]. During training, the model stochastically switches between using the ground-truth CPP and its own predicted CPP for the previous time steps. Initially, the ground-truth values are used most of the time, but as training progresses, the probability of relying on the model's predictions increases. This gradual transition reduces exposure bias and better aligns the model with real-world deployment conditions, where the true CPP values are unknown and must be estimated from PPG and ECG signals. By integrating scheduled sampling, we ensure the model's performance is more representative of actual clinical scenarios.

3.6 Model Selection

After constructing the input modalities, we evaluated various ML models grouped into three categories: classical ML, general DL, and time-series–oriented DL models. These differ in their ability to capture temporal patterns, feature interactions, and data complexity. By assessing their performance with animal-based splitting, we identified the models and input modalities that generalize best to new subjects under realistic clinical conditions.

3.6.1 Classical Machine Learning Models

Classical ML models, such as support vector regression (SVR), random forests (RF), k-nearest neighbors (KNN), and gradient boosted regression trees (GBRT), were chosen for their simplicity and computational efficiency. These models are effective when data are well-preprocessed and feature dimensions are manageable.

Support Vector Regression (SVR)

SVR extends the principles of Support Vector Machines (SVM) to regression tasks. It builds a linear or nonlinear function in a high-dimensional feature space to fit the data within a certain margin of tolerance, and aims to minimize the error while also controlling model complexity through regularization.

Random Forest (RF)

Random Forest is an ensemble learning method that builds multiple decision trees using randomly selected subsets of features and training samples. For regression tasks, the final prediction is obtained by averaging the outputs of all individual trees. This approach reduces variance and enhances predictive accuracy compared to a single decision tree, making it robust against overfitting.

K-Nearest Neighbors (KNN)

KNN is a non-parametric algorithm that predicts the output for a given input by averaging the target values of the k closest training samples in the feature space. The choice of k and the distance metric significantly influence the model's performance, as they determine the neighbors considered for prediction.

Gradient Boosted Regression Trees (GBRT)

GBRT is an iterative ensemble technique that builds a sequence of decision trees, where each subsequent tree aims to correct the residual errors of the combined ensemble of previous trees. By

focusing on the mistakes of prior models, GBRT effectively minimizes the loss function, often leading to high predictive accuracy. However, it requires careful tuning of hyperparameters to prevent overfitting.

3.6.2 General Deep Learning Models

In this category, we evaluate two architectures: the multilayer perceptron (MLP) and the convolutional neural network (CNN). The models are trained using the Adam optimizer with a learning rate of 0.0001 and mean squared error (MSE) as the loss function.

Multilayer Perceptron (MLP)

The MLP model processes each input as a flattened feature vector. It features two fully connected hidden layers with 128 neurons and ReLU activation, followed by batch normalization to stabilize training. Dropout with a rate of 0.2 is applied after each normalization layer to reduce overfitting. The output layer consists of a single linear neuron to estimate CPP values. Although straightforward and efficient to train, MLPs lack the ability to capture long-term dependencies, limiting their effectiveness for sequence data. The architecture is shown in Figure 3.3.

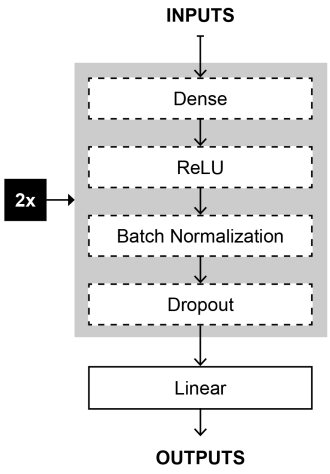

Figure 3.3: Multilayer perceptron (MLP) architecture

Convolutional Neural Network (CNN)

CNNs excel at extracting hierarchical features from input data. Here, we use a one-dimensional CNN to handle time-series data (such as PPG and ECG signals). The architecture includes two Conv1D blocks with 64 and 128 filters, respectively, each using a kernel size of 3 and ReLU activation. Max pooling (pool size of 2), batch normalization, and dropout rate of 0.3 follow each block. The feature maps are then flattened and passed through dense layers of 128 and 64 neurons with ReLU activation and a dropout rate of 0.4 before the single-neuron output layer. The architecture is shown in Figure 3.4.

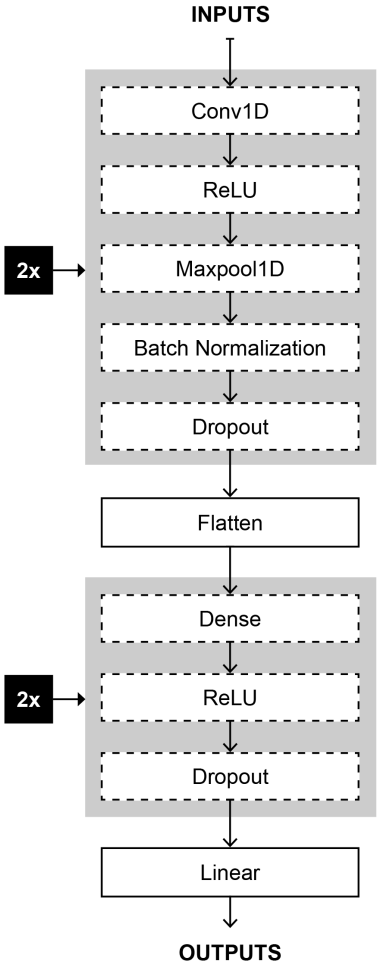

Figure 3.4: Convolutional neural network (CNN) architecture

3.6.3 Time Series-oriented Deep Learning Models

For the stacked multi-cycle input modality, which is a two-dimensional representation encoding information from previous CDCs to predict the CPP value for the next CDC, we leverage advanced time-series architectures, as sequential context is crucial. These include bidirectional Gated Recurrent Units (BiGRU), a hybrid BiGRU–CNN model, sequence-to-sequence (Seq2Seq) models (both with and without attention mechanisms), and transformer networks. Each of these architectures is specifically designed to capture temporal dependencies and contextual relationships within the data. The models are trained using the Adam optimizer with a learning rate of 0.0001 and mean squared error (MSE) as the loss function.

Bidirectional Gated Recurrent Unit (BiGRU)

GRUs are a type of recurrent neural network (RNN) that capture temporal dependencies in sequential data. In a bidirectional setup [54], the network processes the input sequence in both forward and backward directions, merging both hidden states to form the final comprehensive representation. This allows the model to learn past and future context more effectively. Our BiGRU model comprises three stacked bidirectional GRU layers with hidden sizes of 256, 128, and 64, followed by a final bidirectional GRU layer that outputs a 64-dimensional hidden state. Batch normalization and dropout (rate 0.3) are applied after each layer to enhance stability and prevent overfitting. A linear output layer predicts the CPP value. This architecture is highly effective at capturing temporal patterns in PPG and ECG waveforms. An overview of the this model is provided in Figure 3.5.

Bidirectional GRU-CNN (BiGRU-CNN)

The BiGRU-CNN model integrates recurrent and convolutional layers to capture both temporal and spatial features. Two bidirectional GRU layers with hidden sizes of 256 and 128 extract temporal patterns, followed by two CNN blocks with 64 and 128 filters (kernel size 3) and MaxPool1D (pool size 2) for local feature extraction. Dropout (rate 0.3) is applied after each GRU and CNN block to prevent overfitting. A global average pooling layer reduces the feature maps, which are further processed through two fully connected layers with 128 and 64 neurons. The final output

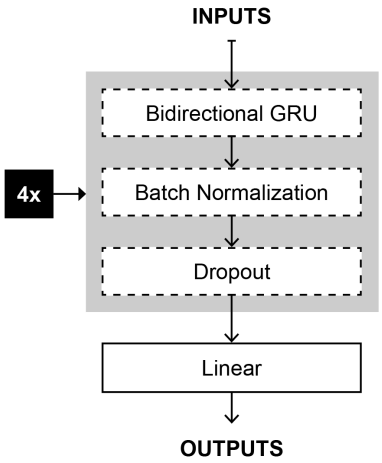

Figure 3.5: BiGRU architecture

layer predicts the CPP value. The architecture is illustrated in Figure 3.6.

Sequence-to-Sequence (Seq2Seq)

Sequence-to-sequence (Seq2Seq) models were first introduced by Sutskever et al. [55] for neural machine translation and have since become foundational in many sequence modeling tasks. A sequence-to-sequence model consists of an encoder and decoder, often built with GRUs or similar RNN variants. The encoder processes the entire input sequence and condenses its information into a final hidden state, which the decoder uses to generate the output. While originally designed for machine translation, Seq2Seq models are adaptable for regression tasks where future values depend on the entire input sequence. In our implementation, the encoder is a 2-layer bidirectional GRU with a hidden size of 64 and a dropout rate of 0.3, outputting the final hidden state. The decoder is a 2-layer GRU with 0.3 dropout, followed by a fully connected layer that predicts a single value. The model architecture is shown in Figure 3.7.

Sequence-to-Sequence (Seq2Seq) with Attention

One limitation of standard Seq2Seq models is the information bottleneck created when the encoder compresses the entire input sequence into a single fixed-length hidden state. This constraint

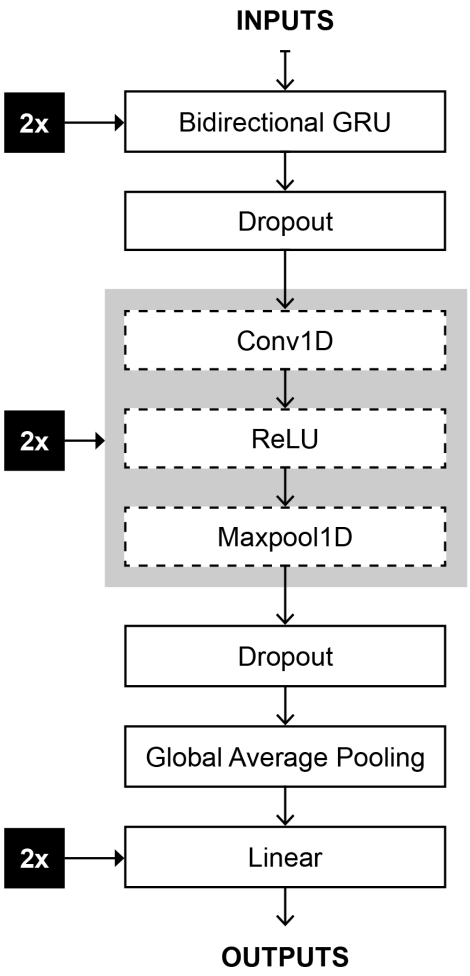

Figure 3.6: BiGRU-CNN architecture

can degrade performance, especially for longer sequences or tasks requiring high temporal precision. To mitigate this issue inherent in the basic sequence-to-sequence framework, we incorporate an attention mechanism inspired by [56] to the basic model. This mechanism enables the decoder to focus on different time steps of the encoder's outputs. The attention layer projects a combination of the encoder's hidden state and the encoder's outputs into a transformed space, computes attention weights, and produces a context vector emphasizing relevant parts of the sequence. This mechanism has proven highly effective in various domains, especially where the relationship between input and output is temporally or spatially complex.

The encoder architecture remains a 2-layer, bidirectional GRU with 0.3 dropout, while the decoder is a 2-layer GRU with 0.3 dropout, enhanced by attention. This refined mechanism pinpoints

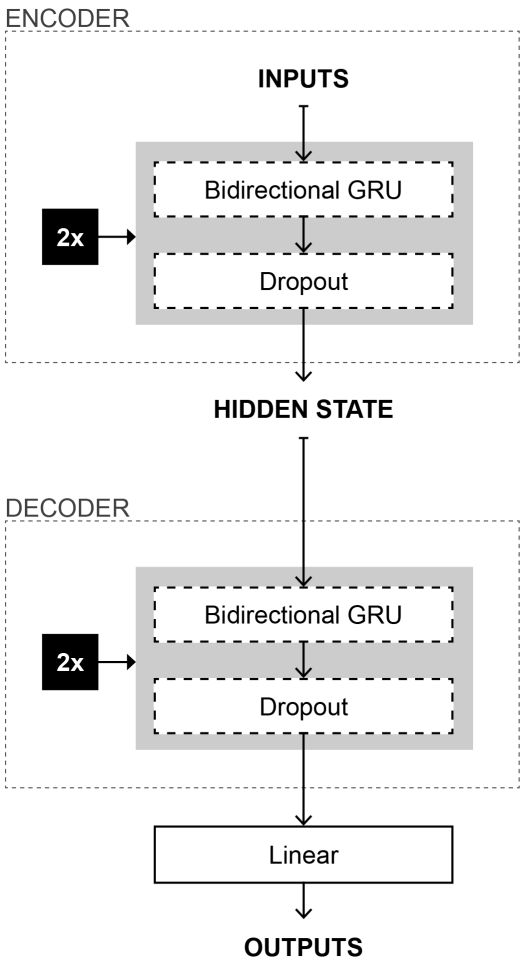

Figure 3.7: Sequence to sequence model architecture

crucial segments in the PPG or ECG signal, improving the model's performance. A graphical representation of this model can be found in Figure 3.7.

Transformer

The Transformer architecture builds upon the foundation established in "Attention Is All You Need" [57], replacing recurrent modules with multi-head self-attention. Transformers have been widely adopted in natural language processing and have recently demonstrated strong performance in various domains including time-series applications.

Unlike recurrent neural networks (RNNs) and their variants (e.g., LSTMs and GRUs), which

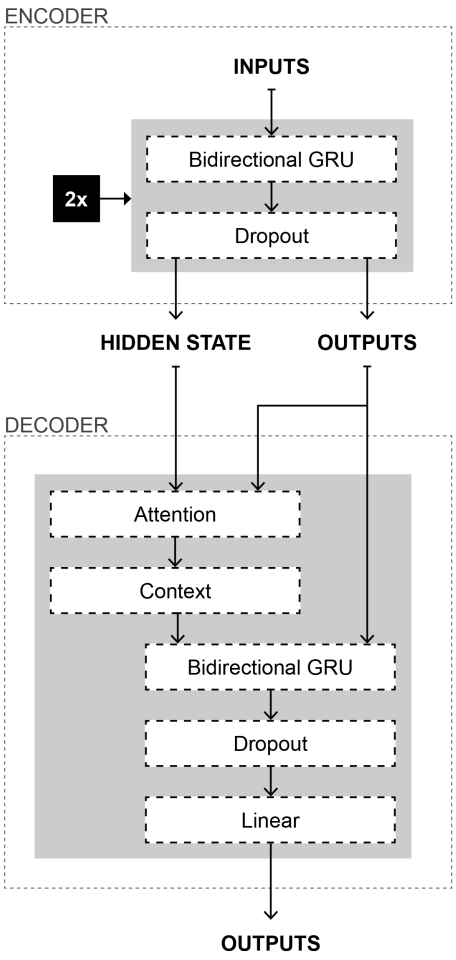

Figure 3.8: Sequence to sequence with attention model architecture

process input sequences sequentially, the Transformer processes entire sequences in parallel using self-attention mechanisms. This design enables the model to capture long-range dependencies more effectively and allows for greater computational efficiency, particularly beneficial for time-series data where patterns can span extensive temporal intervals.

In our implementation, an embedding layer of size 128 projects the input features into a higher-dimensional space. Six Transformer encoder layers, each with eight attention heads and a feed-forward sublayer (internal dimension 128), capture both local and global dependencies. Layer normalization and residual connections stabilize training. A final projection layer flattens the sequence and outputs the predicted CPP. The model structure is shown in Figure 3.9.

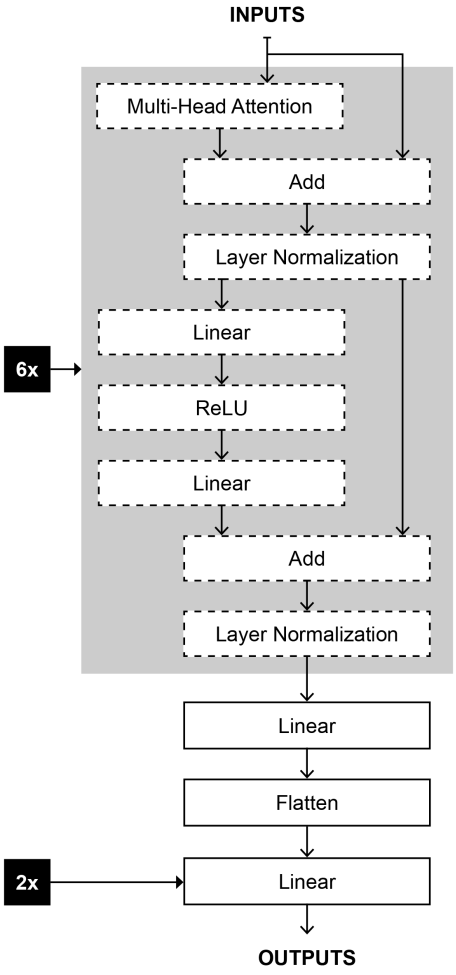

Figure 3.9: Transformer model architecture

3.6.4 Evaluation Scenarios and Input Configurations

To systematically evaluate the performance of the models, we define two distinct experimental scenarios based on the presence or absence of ROSC in the subjects.

(1) **ROSC-only Ccenario:** Models are trained and tested exclusively on data from animals who achieved ROSC.

(2) **Mixed ROSC/non-ROSC Scenario:** Models are trained and tested on a combined dataset that includes animals who did and did not achieve ROSC.

The separation of these scenarios is motivated by the distinct physiological patterns observed

in animals with and without ROSC. Animals achieving ROSC typically exhibit higher and more stable coronary perfusion pressure (CPP) values. Conversely, non-ROSC animals often display persistently low CPP, irregular waveforms, or abrupt signal drops caused by sustained cardiac arrest [4]. Analyzing both scenarios allows us to assess the models' ability to generalize across different clinical outcomes and data distributions. In this study, ROSC is defined as the return of spontaneous circulation for more than 30 seconds, as outlined in the Utstein guidelines for uniform reporting in animal cardiopulmonary research [58].

Within each scenario, we examine three configurations of input signals: PPG alone, ECG alone, and a combined PPG+ECG input. Studying these configurations enables us to identify the contribution of each signal modality to predictive performance and to determine whether multi-modal data can further enhance model accuracy.

Chapter 4

Results

This section presents the results obtained using the three input modalities: single-cycle, rolling-window multi-cycle, and stacked multi-cycle. Each modality is evaluated with both classical machine learning and deep learning models, as introduced in 3.6. The analysis is conducted across two distinct experimental scenarios, ROSC-only and mixed ROSC/non-ROSC, using three configurations: PPG alone, ECG alone, and a combined PPG and ECG. Performance is evaluated based on mean absolute error (MAE), standard deviation error (SDE), and Pearson correlation coefficient (r-value).

4.1 Single-Cycle Input Modality

Table 4.1 presents the performance results under the single-cycle input modality, where each compression–decompression cycle is evaluated independently. In this setting, models are trained using only local (per-cycle) information without explicitly leveraging any temporal continuity across cycles.

For the ROSC scenario, utilizing ECG data alone generally results in slightly higher errors and lower correlations compared to PPG-only inputs, which exhibit more robust performance. Furthermore, combining PPG and ECG does not consistently improve outcomes across all models; some show marginal improvements, while others perform slightly worse. This suggests that, for the ROSC scenario, the inclusion of ECG signals does not offer significant advantages.

Table 4.1: Performance results using the single-cycle input modality, comparing results for ROSC-only and mixed ROSC/non-ROSC group. Results are reported separately for models trained on PPG alone, ECG alone, and combined PPG+ECG signals.

Model	ROSC-only group			Mixed group (ROSC/non-ROSC)		
	MAE (mmHg)	SDE (mmHg)	r-value	MAE (mmHg)	SDE (mmHg)	r-value
PPG Signals Only						
SVR	**7.40**	**7.18**	**0.39**	8.87	7.60	0.07
RF	7.48	7.31	0.42	8.76	7.41	0.12
KNN	8.09	8.05	0.36	9.21	8.28	0.07
GBRT	7.41	7.08	0.45	8.48	7.12	0.11
MLP	7.07	6.71	0.46	**8.16**	**6.80**	**0.18**
CNN	8.32	6.53	0.49	8.88	7.20	0.02
ECG Signals Only						
SVR	**7.35**	**7.32**	**0.25**	**7.48**	**6.54**	**0.19**
RF	7.77	7.25	0.33	7.45	6.59	0.18
KNN	8.36	7.55	0.34	7.72	6.93	0.19
GBRT	8.30	7.85	0.27	7.72	6.69	0.16
MLP	9.87	7.99	0.28	8.08	7.06	0.15
CNN	8.97	7.82	0.20	8.61	6.80	0.17
PPG and ECG Signals Together						
SVR	**7.31**	**7.44**	**0.26**	**7.52**	**6.56**	**0.15**
RF	7.42	6.93	0.47	8.22	6.78	0.20
KNN	7.84	7.10	0.47	8.05	7.37	0.20
GBRT	7.56	6.98	0.46	8.11	6.89	0.19
MLP	7.66	6.86	0.52	8.28	7.16	0.17
CNN	8.91	6.56	0.48	9.78	6.73	0.19

In scenarios involving mixed ROSC/non-ROSC group of animals, models tend to achieve better results when utilizing ECG alone rather than relying solely on PPG or a combination of PPG and ECG. This indicates that ECG data can provide valuable information in cases involving mixed ROSC/non-ROSC animal populations.

The best model for the ROSC scenario is a SVR model using a combination of PPG and ECG waveforms and achieving a MAE of 7.31 mmHg, a SDE of 7.44 mmHg, and a r-value of 0.26. For the mixed ROSC/non-ROSC group scenario, the best performance is observed with a RF model

using ECG alone, which achieves a MAE of 7.45 mmHg, a SDE of 6.59 mmHg, and a r-value of 0.18. Despite the r-value differences, the two scenarios show comparable results in terms of MAE and SDE. Overall, comparing the ROSC-only group to the mixed ROSC/non-ROSC group reveals that r-values are generally higher for ROSC group. This outcome is likely due to the relative stability of ROSC group, characterized by higher and more consistent CPP values and consistent CPP waveform trends. In contrast, non-ROSC recordings exhibit significant variability and lower perfusion pressures, contributing to reduced correlations.

4.2 Rolling-Window Multi-Cycle Input Modality

Table 4.2 provides the results for the rolling-window multi-cycle modality, where sequences of consecutive compression–decompression cycles are used as input. Each window captures local temporal dependencies, and overlapping segments are created by shifting the window by one cycle. For each window, the target CPP is defined as the average of the peak CPP values across all cycles contained within the window. Overall, this approach yields lower mean absolute errors (MAE) and higher Pearson correlation coefficients (r-value) compared to the single-cycle setting, highlighting the importance of incorporating temporal information for capturing CPP dynamics more effectively.

For the ROSC group, models utilizing only PPG waveforms outperform those using ECG alone or a combination of PPG and ECG. This suggests that for ROSC-only group, ECG signals do not provide additional information beyond what is captured by PPG signals in terms of CPP waveform representation.

In contrast, for the mixed ROSC/non-ROSC group, models trained on ECG-alone data perform better on average than those using only PPG. Furthermore, models that leverage both PPG and ECG together achieve the best results for this group. This indicates that while PPG signals alone are sufficient to represent CPP waveforms in the ROSC group, ECG signals play a more critical role in accurately estimating CPP waveforms in non-ROSC scenarios, where greater variability in physiological patterns is observed.

The best model for the ROSC group is the MLP trained on PPG data, achieving a MAE of 5.93 mmHg, a SDE of 5.59 mmHg, and a r-value of 0.61. For the mixed ROSC/non-ROSC group, the

Table 4.2: Performance results using the rolling-window multi-cycle input modality, comparing results for ROSC-only and mixed ROSC/non-ROSC group. Results are reported separately for models trained on PPG alone, ECG alone, and combined PPG+ECG signals.

Model	ROSC-only group			Mixed group (ROSC/non-ROSC)		
	MAE (mmHg)	SDE (mmHg)	r-value	MAE (mmHg)	SDE (mmHg)	r-value
PPG Signals Only						
SVR	6.73	6.11	0.48	8.49	7.09	0.10
RF	7.03	6.18	0.52	8.47	6.79	0.15
KNN	7.85	7.49	0.40	9.22	8.27	0.07
GBRT	7.01	6.20	0.52	**8.41**	**6.67**	**0.14**
MLP	**5.93**	**5.59**	**0.61**	9.12	6.35	0.15
CNN	6.73	6.21	0.48	9.76	6.65	0.14
ECG Signals Only						
SVR	8.46	7.22	0.23	8.05	6.21	0.18
RF	**7.93**	**6.68**	**0.39**	**7.87**	**6.09**	**0.20**
KNN	8.94	7.37	0.26	8.52	6.97	0.12
GBRT	8.77	7.36	0.33	8.22	6.35	0.16
MLP	9.09	6.66	0.43	8.42	6.89	0.01
CNN	8.28	6.48	0.35	9.53	6.54	0.14
PPG and ECG Signals Together						
SVR	**6.97**	**6.63**	**0.39**	**7.37**	**6.32**	**0.13**
RF	7.08	5.88	0.56	8.18	6.31	0.19
KNN	8.24	6.98	0.48	8.94	7.80	0.16
GBRT	7.41	5.98	0.56	8.44	6.64	0.15
MLP	7.49	6.51	0.55	7.89	6.29	0.24
CNN	7.79	5.52	0.60	9.24	6.09	0.25

best performance is achieved using both PPG and ECG signals with the SVR model, yielding a MAE of 7.37 mmHg, a SDE of 6.32 mmHg, and a r-value of 0.13.

As observed in earlier input modalities analysis, the ROSC-only group achieves better performance metrics overall due to the more consistent and stable physiological patterns present in their data. Nevertheless, certain models demonstrate satisfactory accuracy in the mixed ROSC/non-ROSC scenario, suggesting robustness in handling the increased variability within this dataset.

4.3 Stacked Multi-Cycle Input Modality

Table 4.3 summarizes the performance of our stacked multi-cycle input modality, where multiple consecutive cycles are vertically concatenated into a 2D array. This data structure is particularly suitable for sequence-based architectures such as BiGRU, Seq2Seq with/without attention, Transformers and hybrid models like BiGRU–CNN. The target CPP is defined as the maximum CPP value in the subsequent cycle, reflecting the clinical need to predict and respond to future CPP levels during CPR in real-time.

Table 4.3: Performance results using the stacked multi-cycle input modality, comparing results for ROSC-only and mixed ROSC/non-ROSC group. Results are reported separately for models trained on PPG alone, ECG alone, and combined PPG+ECG signals.

Model	**ROSC-only group**			**Mixed group (ROSC/non-ROSC)**		
	MAE (mmHg)	**SDE (mmHg)**	**r-value**	**MAE (mmHg)**	**SDE (mmHg)**	**r-value**
PPG Signals Only						
BiGRU	7.56	6.96	0.55	8.80	7.14	0.07
BiGRU-CNN	**6.75**	**6.27**	**0.56**	7.77	6.08	0.30
Seq2Seq	6.79	6.30	0.56	7.83	6.11	0.30
Seq2Seq with Attention	6.85	6.28	0.56	7.89	6.05	0.32
Transformer	7.10	6.53	0.56	**7.74**	**6.61**	**0.20**
ECG Signals Only						
BiGRU	10.02	8.20	0.30	8.86	6.84	0.08
BiGRU-CNN	8.07	7.07	0.39	7.54	6.52	0.04
Seq2Seq	7.59	7.05	0.38	7.70	6.45	0.07
Seq2Seq with Attention	**7.485**	**6.89**	**0.41**	7.56	6.42	0.10
Transformer	7.95	7.48	0.35	**7.13**	**6.99**	**0.23**
PPG and ECG Signals Together						
BiGRU	8.23	7.55	0.52	8.56	7.47	0.14
BiGRU-CNN	7.30	6.38	0.57	7.31	6.14	0.24
Seq2Seq	7.03	6.33	0.57	7.87	6.20	0.27
Seq2Seq with Attention	**6.91**	**6.26**	**0.57**	8.01	6.20	0.27
Transformer	7.00	5.96	0.59	**6.41**	**6.58**	**0.35**

In the ROSC setting using PPG-only inputs, the BiGRU–CNN model achieves the highest accuracy, with a MAE of 6.75 mmHg, a SDE of 6.27 mmHg, and a r-value of 0.56. This finding highlights the benefit of combining recurrent layers (for temporal dependencies) with convolutional filters (for local waveform patterns). For ECG-only inputs, the Seq2Seq model with attention yields

the best result (MAE of 7.48 mmHg, a SDE of 6.89 mmHg, and a r-value of 0.41), while combining both PPG and ECG waveforms again favors the Seq2Seq model with attention (MAE of 6.91 mmHg, a SDE of 6.26 mmHg, and a r-value of 0.57). Averaging across all architectures, PPG-only inputs perform best, followed by PPG+ECG, and finally ECG-only, underscoring PPG's importance in predicting CPP trends in ROSC cases.

In the mixed group (ROSC/non-ROSC), the Transformer model achieves the best performance when combining PPG and ECG inputs, with a MAE of 6.41 mmHg, a SDE of 6.58 mmHg, and a r-value of 0.35. This surpasses any single-modality results from the ROSC-only group, demonstrating the benefit of integrating ECG signals for heterogeneous populations. For ECG-only inputs, the Transformer achieves better performance (MAE = 7.13 mmHg, SDE = 6.99 mmHg, r = 0.23) compared to PPG-only (MAE = 7.74 mmHg, SDE = 6.61 mmHg, r = 0.20). This suggests that ECG waveforms provide additional physiological context, particularly for non-ROSC animals.

Overall, PPG signals alone are sufficient for predicting CPP in strictly ROSC scenarios. However, in more diverse populations (mixed ROSC/non-ROSC), combining PPG and ECG inputs proves superior, with the Transformer model emerging as the top performer. This highlights the value of additional physiological information captured by ECG signals in enhancing model performance for heterogeneous datasets.

Moreover, the Transformer model performs better in the mixed ROSC/non-ROSC scenario than in the ROSC-only scenario, a finding unique to the stacked multi-cycle approach. This outcome was not observed with previous models or input modalities. The stacked multi-cycle design, combined with the Transformer's attention mechanism, enables the model to capture essential features across a diverse population rather than being limited to a specific subset. This robustness in predicting future CPP values underscores the potential of this approach in real-world settings, where animal conditions can vary widely.

In Figure 4.1, the boxplot illustrates the performance of various models for the mixed group (ROSC/non-ROSC) using PPG and ECG combined. As previously mentioned, the LOSO evaluation method was employed. In this approach, the model is trained on data from all animals except one, which is then used as the test subject. This process is repeated for every animal in the dataset, and the performance metrics are averaged across all iterations to assess the model's overall generalizability.

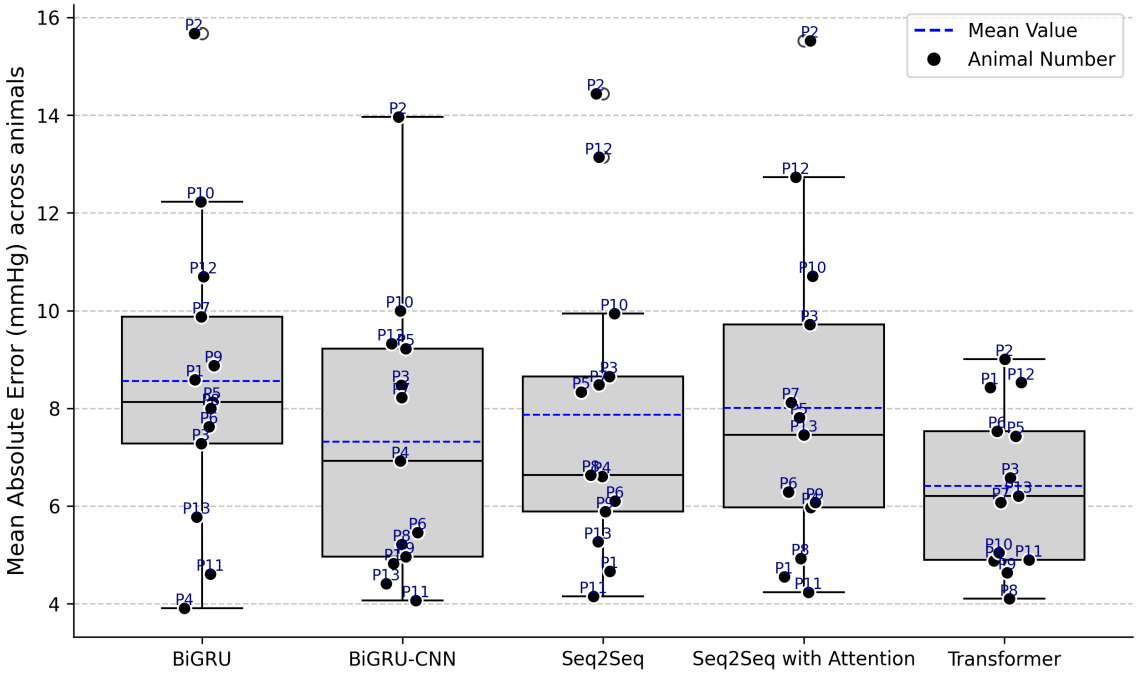

Figure 4.1: Boxplot showing the performance of deep learning models for the mixed group (ROSC/non-ROSC) using combined PPG and ECG signals in the stacked multi-cycle input modality.

The boxplot shows the performance of each model for every animal when used as the test subject. Each point in the boxplot represents the model's performance (in terms of MAE) when a specific animal was used as the test subject. Additionally, the mean value, representing the average MAE across all tests for each model, is displayed. The distribution of these values reflects the variability in performance across different subjects, and the plotted mean denotes the average MAE across all folds for each model. Notably, animals 2 and 12 exhibit significantly poor performance compared to the other models. Consequently, these animals were excluded from the dataset, and the experiment was repeated to evaluate the impact of their removal.

The results of the adjusted experiment, presented in Table 4.4, show that excluding animals 2 and 12 leads to improved performance across all models. The MAE decreases, and the r-values increase significantly, indicating a stronger correlation between predicted and actual CPP values. Among the models, the Transformer achieves the best performance, with a MAE of 6.20 mmHg, a SDE of 6.02 mmHg, and a r-value of 0.42. The sequence-to-sequence model with attention follows closely, yielding a MAE of 6.30 mmHg, a SDE of 5.69 mmHg, and a r-value of 0.38. This result

further confirms the Transformer's ability to capture the complex relationship between PPG, ECG, and CPP values.

Table 4.4: Performance results for the mixed ROSC/non-ROSC group using combined PPG and ECG signals, with outliers removed from the animal dataset.

Model	MAE (mmHg)	SDE (mmHg)	r-value
BiGRU	8.21	6.96	0.24
BiGRU-CNN	6.79	5.94	0.34
Seq2Seq	6.35	5.78	0.36
Seq2Seq with Attention	6.30	5.69	0.38
Transformer	**6.20**	**6.02**	**0.42**

4.4 Comparison of the Performance among Models

In this study, we explored three distinct input modalities, single-cycle, rolling-window multi-cycle, and stacked multi-cycle for predicting CPP during CPR. We assessed a variety of classical machine learning algorithms and deep learning architectures across two experimental scenarios: one focusing solely on the ROSC group of animals and the other encompassing both ROSC and non-ROSC groups.

When evaluating performance across these input modalities, we observed distinct trends based on whether animals achieved ROSC. As shown in Figure 4.2, for the ROSC group, PPG-only inputs generally outperformed both ECG-only inputs and the combination of PPG and ECG. This suggests that, for animals who achieved ROSC, PPG captures the critical information required for accurate CPP prediction, rendering the additional ECG data less impactful. However, the opposite was true for the mixed group: ECG-only inputs performed better than PPG-only, and combining PPG and ECG provided even greater predictive power. Although including ECG improved prediction accuracy in our small sample of 13 pigs, this benefit was not overwhelmingly large. It is possible that with a larger sample size, the performance difference between PPG-only and combined PPG–ECG inputs would grow, potentially justifying the additional steps required.

In terms of modeling approaches, incorporating temporal context significantly enhanced prediction performance. As shown in Figure 4.3 and detailed in Table 4.5, the rolling-window and stacked multi-cycle input modalities yielded better results than single-cycle inputs, highlighting the benefit of capturing a broader temporal context. Sequence-based models, such as Transformer, Seq2Seq with attention and BiGRU–CNN, successfully leveraged these temporal dependencies and outperformed non-time-series architectures. In contrast, the single-cycle approach, which treats each compression–decompression cycle independently, struggled to capture longer-term CPP trends, leading to higher mean absolute error (MAE) values and lower pearson correlation coefficients (r-value).

Table 4.5: Best-performing models and their corresponding mean absolute error (MAE in mmHg) for each combination of input modality (single-cycle, rolling-window, stacked multi-cycle) and signal type (PPG, ECG, PPG+ECG), reported separately for ROSC-only and mixed (ROSC/non-ROSC) groups.

Group	Input Modality	PPG	ECG	PPG + ECG
ROSC	Single-Cycle	MLP (7.07)	SVR (7.35)	SVR (7.31)
	Rolling-Window	MLP (5.93)	RF (7.93)	SVR (6.97)
	Stacked Multi-Cycle	BiGRU-CNN (6.75)	Seq2Seq+Att (7.49)	Seq2Seq+Att (6.91)
Mixed	Single-Cycle	MLP (8.16)	RF (7.45)	SVR (7.52)
	Rolling-Window	MLP (8.16)	BiGRU-CNN (7.54)	SVR (7.37)
	Stacked Multi-Cycle	Transformer (7.74)	Transformer (7.13)	Transformer (6.41)

Another influential factor was dataset composition and sample size. Models trained exclusively on data from the ROSC group performed better than those trained on a mixed set of ROSC and non-ROSC cases. This finding suggests that the more stable physiological patterns characteristic of successful resuscitations yield more accurate predictions. Nevertheless, our dataset's limitation to 13 pigs constrained the generalizability of our analysis. A larger and more diverse data set would mitigate the risks of overfitting, increase the robustness of the model, and potentially reveal subtler performance differences between the two groups. Deep learning techniques, in particular, benefit substantially from increased data volume, often resulting in markedly improved outcomes.

Regarding the best-performing models, the MLP model achieved the strongest results in the ROSC scenario by effectively capturing temporal dependencies. In the mixed group, the transformer model demonstrated the highest accuracy, highlighting its suitability for handling combined

ROSC and non-ROSC data. Based on these insights, future work will focus on enlarging the dataset and further investigating the effect of including ECG alongside PPG. A larger dataset will help verify whether the observed trends persist and whether the performance gap between PPG-only and combined PPG—ECG strategies is significant enough to justify the additional complexity and time required for ECG electrode placement.

Ultimately, our research provides valuable guidance for clinical decision-making concerning noninvasive, real-time, calibration-free CPP monitoring. While including ECG may yield accuracy improvements, especially in non-ROSC scenarios, the practical trade-offs must be weighed carefully, particularly under the urgent conditions of CPR. Expanding the dataset, refining deep learning models, and thoroughly evaluating these approaches in larger studies will be key steps in advancing this field and improving animal outcomes.

In summary, this chapter presented a comprehensive evaluation of CPP prediction using three different input modalities: single-cycle, rolling-window multi-cycle, and stacked multi-cycle. A variety of classical and deep learning models were applied to assess how temporal context influences estimation accuracy. The results demonstrated that incorporating multi-cycle temporal information leads to more accurate CPP predictions than using single-cycle inputs. Among all configurations, the stacked multi-cycle input combined with transformer-based models and scheduled sampling achieved the highest performance, highlighting the importance of attention mechanisms and temporal modeling in capturing the complex dynamics of CPR.

The analysis also highlighted that the choice of signal modality influences model performance depending on the clinical context. In ROSC cases, PPG signals alone were sufficient for accurate CPP estimation. However, combining PPG and ECG improved performance in mixed ROSC and non-ROSC scenarios, where physiological variability is higher. These findings suggest that the inclusion of ECG may be beneficial in more complex cases, although its use should be weighed against added system complexity and data acquisition constraints.

Overall, this chapter provides strong empirical support for the feasibility of real-time, non-invasive CPP estimation using raw physiological signals and machine learning. The next chapter concludes the thesis by summarizing the key contributions and outlining directions for future research and clinical application.

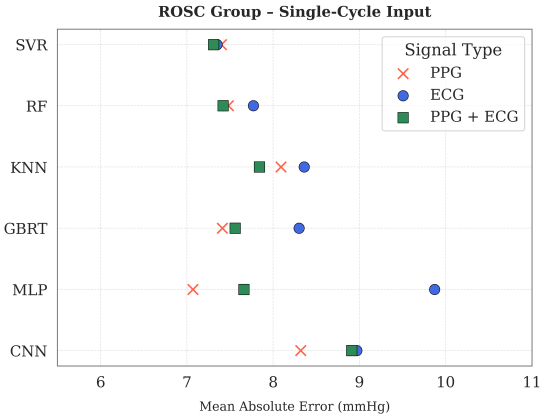

ROSC-only: Single-Cycle

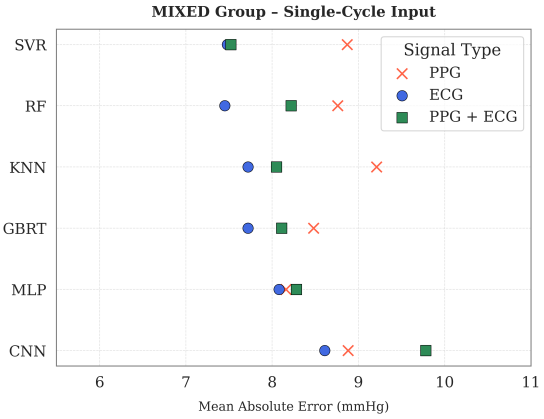

Mixed: Single-Cycle

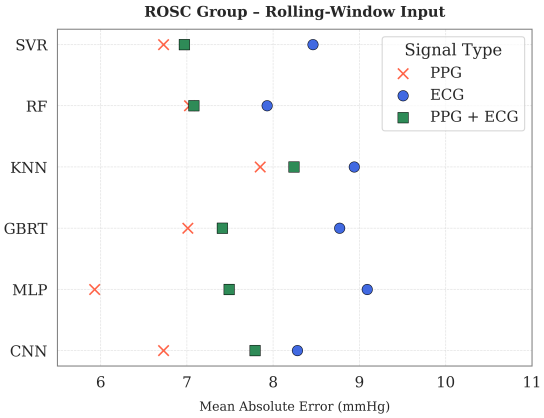

ROSC-only: Rolling-Window

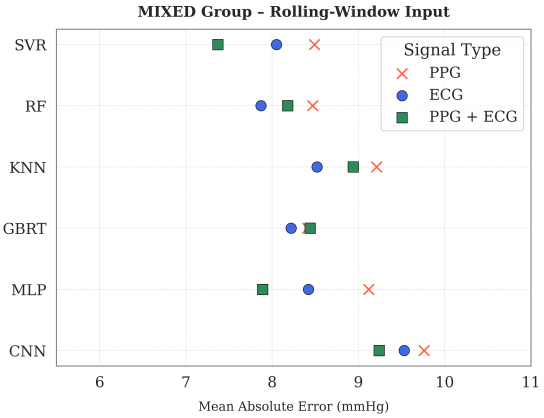

Mixed: Rolling-Window

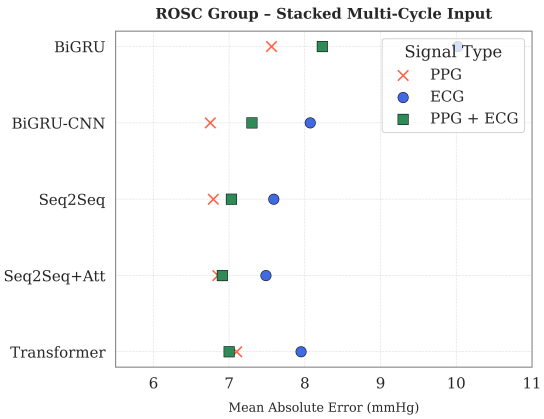

ROSC-only: Stacked Multi-Cycle

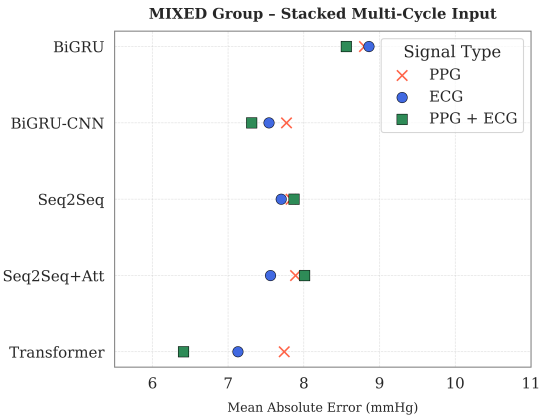

Mixed: Stacked Multi-Cycle

Figure 4.2: Comparison of mean absolute error (MAE) values for various machine learning models across three input modalities and two groups: ROSC-only and mixed (ROSC/non-ROSC). Each point represents the MAE obtained by a specific model using either PPG, ECG, or combined PPG+ECG signals.

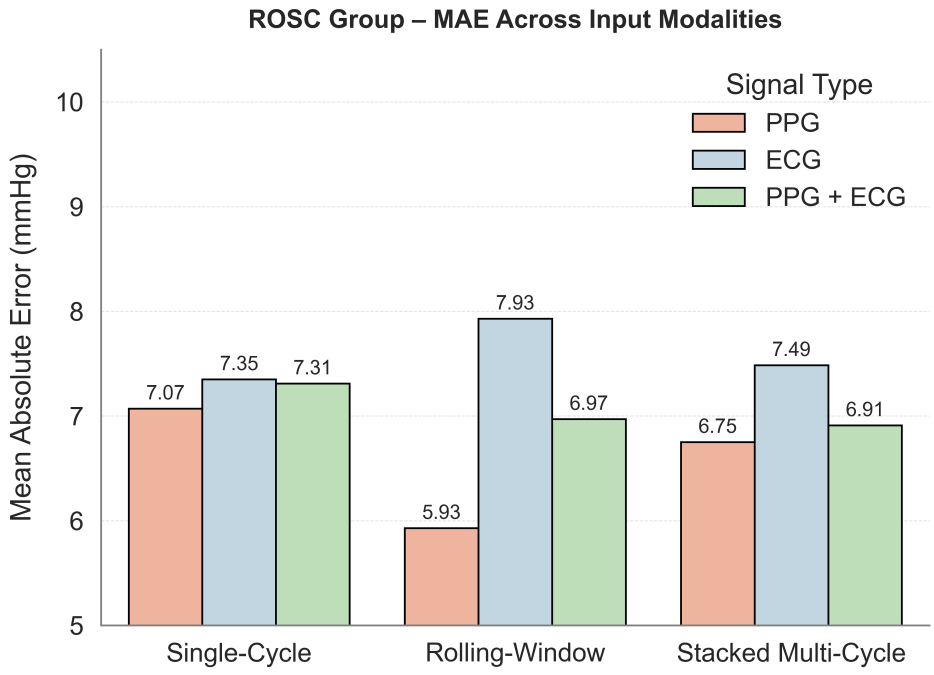

(a) ROSC-only group

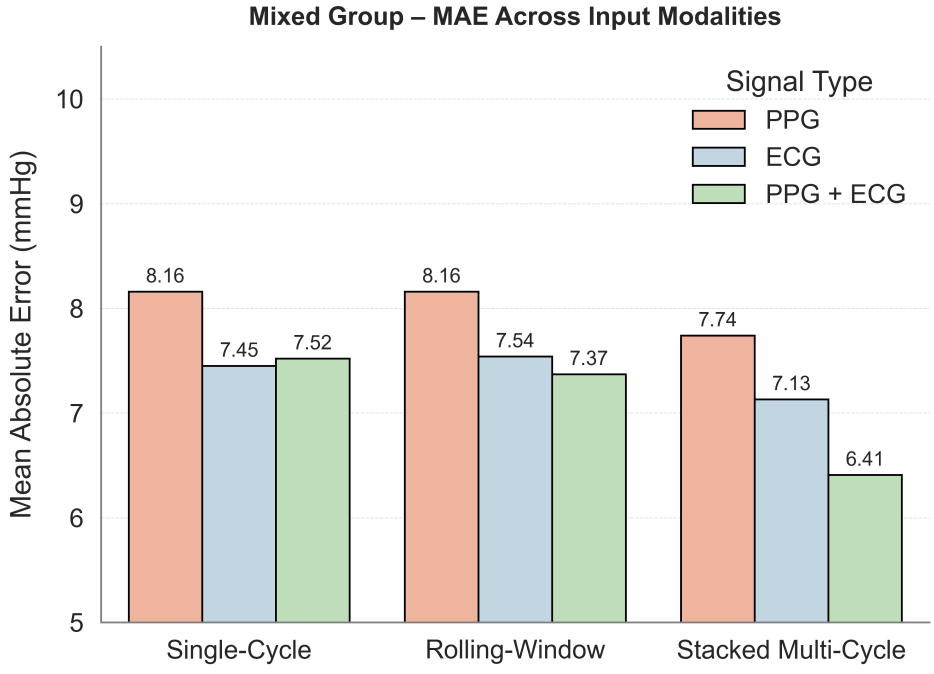

(b) Mixed (ROSC/non-ROSC) group

Figure 4.3: Best-performing models (based on lowest MAE) for each combination of input modalities (single-cycle, rolling-window, stacked multi-cycle) and signal types (PPG, ECG, PPG+ECG) in both ROSC-only and mixed (ROSC/non-ROSC) groups.

Chapter 5

Conclusion

5.1 Discussion

This thesis presented a novel machine learning–based framework for real-time, continuous, non-invasive, and calibration-free estimation of CPP during CPR. By leveraging raw PPG and ECG signals, the proposed system enables individualized, data-driven optimization of CPR delivery, with the goal of enhancing myocardial perfusion and improving ROSC outcomes.

To fully exploit temporal and spectral characteristics of physiological waveforms, three distinct input modalities were investigated: single-cycle, rolling-window multi-cycle, and stacked multi-cycle representations. Experimental results demonstrated that incorporating temporal context significantly improves prediction accuracy, with the stacked multi-cycle modality—particularly when paired with attention-based Transformer models, yielding the best performance. Additionally, the study highlighted the utility of scheduled sampling as a training strategy for improving generalization and robustness, especially under animal-split testing conditions.

The comparative analysis across various models, including classical machine learning models (e.g., SVR, RF, KNN, GBRT), deep learning models (e.g., MLPs, CNNs), and time-series architectures (e.g., BiGRUs, Seq2Seq, Transformers), enabled a comprehensive evaluation of the proposed framework under realistic CPR conditions. Findings indicate that PPG signals alone often suffice for accurate CPP estimation in ROSC cases, while combining PPG and ECG improves prediction performance in non-ROSC scenarios. However, the clinical utility of including ECG should be

carefully weighed against the additional complexity it introduces.

Despite promising outcomes, the study's small dataset highlights the need for larger, more diverse samples to validate findings and improve generalizability. In summary, this work contributes to the growing body of research on intelligent, physiologically guided CPR by introducing and validating a non-invasive, calibration-free CPP estimation framework. By providing real-time, actionable feedback during resuscitation, the proposed system has the potential to transform CPR from a generalized protocol into a personalized intervention, thereby improving survival outcomes during cardiac arrest.

5.2 Future Work

While this study presents a promising framework for non-invasive CPP estimation during CPR, several important directions remain for future research. A primary limitation of the current work is the relatively small dataset, which constrains the generalizability of the findings. Expanding the dataset to include larger and more diverse samples across subjects, conditions, and physiological variations is essential to enhance model robustness and support broader clinical applicability.

Future research could explore domain adaptation and transfer learning techniques to enable cross-subject or cross-species generalization without the need for retraining from scratch. Incorporating additional physiological signals such as end-tidal CO_2, compression force, or accelerometer data from CPR devices, may further enrich the input representation and improve estimation accuracy. Contextual data such as rescuer feedback and real-time compression quality metrics could also enhance model adaptability in dynamic resuscitation settings.

Another promising direction involves closing the feedback loop between CPP estimation and CPR delivery. If real-time data on compression depth, rate, and hand placement are available, reinforcement learning could be leveraged to learn optimal CPR strategies that adapt dynamically to real-time estimated CPP. This would enable a fully adaptive system where CPR parameters are continuously adjusted in response to physiological feedback, potentially leading to improved perfusion and survival outcomes.

Finally, validating the proposed system in real-time experimental settings, both in pre-clinical

animal models and clinical environments will be critical for translating this research into practice. Deployment studies should assess latency, reliability, and usability of the system under realistic conditions to evaluate its feasibility as a decision support tool for personalized, physiologically guided CPR, bringing this framework closer to practical and lifesaving application.

Bibliography

[1] P. A. Meaney, B. J. Bobrow, M. E. Mancini, J. Christenson, A. R. De Caen, F. Bhanji, B. S. Abella, M. E. Kleinman, D. P. Edelson, R. A. Berg *et al.*, "Cardiopulmonary resuscitation quality: improving cardiac resuscitation outcomes both inside and outside the hospital: a consensus statement from the american heart association," *circulation*, vol. 128, no. 4, pp. 417–435, 2013.

[2] J. T. Niemann, J. P. Rosborough, S. Ung, and J. M. Criley, "Coronary perfusion pressure during experimental cardiopulmonary resuscitation," *Annals of emergency medicine*, vol. 11, no. 3, pp. 127–131, 1982.

[3] J. Xu, H. Zhu, Z. Wang, X. Yu, and J. Walline, "Why do not we use finger pulse oximeter plethysmograph waveform to monitor the effectiveness of cardiopulmonary resuscitation?" *Resuscitation*, vol. 82, no. 7, pp. 959–959, 2011.

[4] J. C. Reynolds, D. D. Salcido, and J. J. Menegazzi, "Correlation between coronary perfusion pressure and quantitative ecg waveform measures during resuscitation of prolonged ventricular fibrillation," *Resuscitation*, vol. 83, no. 12, pp. 1497–1502, 2012.

[5] F. Zuo, Y. Ding, C. Dai, L. Wei, Y. Gong, J. Wang, Y. Shen, and Y. Li, "Estimating the amplitude spectrum area of ventricular fibrillation during cardiopulmonary resuscitation using only ecg waveform," *Annals of Translational Medicine*, vol. 9, no. 8, 2021.

[6] D. D. Salcido, Y.-M. Kim, L. D. Sherman, G. Housler, X. Teng, E. S. Logue, and J. J. Menegazzi, "Quantitative waveform measures of the electrocardiogram as continuous physiologic feedback during resuscitation with cardiopulmonary bypass," *Resuscitation*, vol. 83,

no. 4, pp. 505–510, 2012.

[7] Y. Azeli, J. V. Lorente Olazabal, M. I. Monge García, and A. Bardají, "Understanding the adverse hemodynamic effects of serious thoracic injuries during cardiopulmonary resuscitation: a review and approach based on the campbell diagram," *Frontiers in physiology*, vol. 10, p. 500823, 2019.

[8] S. H. Ralston, W. D. Voorhees, and C. F. Babbs, "Intrapulmonary epinephrine during prolonged cardiopulmonary resuscitation: improved regional blood flow and resuscitation in dogs," *Annals of emergency medicine*, vol. 13, no. 2, pp. 79–86, 1984.

[9] H. R. Halperin, J. E. Tsitlik, A. D. Guerci, E. Mellits, H. Levin, A.-Y. Shi, N. Chandra, and M. Weisfeldt, "Determinants of blood flow to vital organs during cardiopulmonary resuscitation in dogs." *Circulation*, vol. 73, no. 3, pp. 539–550, 1986.

[10] S. Rubertsson and R. Karlsten, "Increased cortical cerebral blood flow with lucas; a new device for mechanical chest compressions compared to standard external compressions during experimental cardiopulmonary resuscitation," *Resuscitation*, vol. 65, no. 3, pp. 357–363, 2005.

[11] A. S. Go, D. Mozaffarian, V. L. Roger, E. J. Benjamin, J. D. Berry, W. B. Borden, D. M. Bravata, S. Dai, E. S. Ford, C. S. Fox *et al.*, "Heart disease and stroke statistics—2013 update: a report from the american heart association," *circulation*, vol. 127, no. 1, pp. e6–e245, 2013.

[12] P. S. Chan, B. McNally, F. Tang, and A. Kellermann, "Recent trends in survival from out-of-hospital cardiac arrest in the united states," *Circulation*, vol. 130, no. 21, pp. 1876–1882, 2014.

[13] S. Yan, Y. Gan, N. Jiang, R. Wang, Y. Chen, Z. Luo, Q. Zong, S. Chen, and C. Lv, "The global survival rate among adult out-of-hospital cardiac arrest patients who received cardiopulmonary resuscitation: a systematic review and meta-analysis," *Critical care*, vol. 24, pp. 1–13, 2020.

[14] M. P. Larsen, M. S. Eisenberg, R. O. Cummins, and A. P. Hallstrom, "Predicting survival from out-of-hospital cardiac arrest: a graphic model," *Annals of emergency medicine*, vol. 22, no. 11, pp. 1652–1658, 1993.

[15] S. Rubertsson, E. Lindgren, D. Smekal, O. Östlund, J. Silfverstolpe, R. A. Lichtveld, R. Boomars, B. Ahlstedt, G. Skoog, R. Kastberg *et al.*, "Mechanical chest compressions and simultaneous defibrillation vs conventional cardiopulmonary resuscitation in out-of-hospital cardiac arrest: the linc randomized trial," *Jama*, vol. 311, no. 1, pp. 53–61, 2014.

[16] J. Shin, J. E. Rhee, and K. Kim, "Is the inter-nipple line the correct hand position for effective chest compression in adult cardiopulmonary resuscitation?" *Resuscitation*, vol. 75, no. 2, pp. 305–310, 2007.

[17] N. A. Paradis, G. B. Martin, E. P. Rivers, M. G. Goetting, T. J. Appleton, M. Feingold, and R. M. Nowak, "Coronary perfusion pressure and the return of spontaneous circulation in human cardiopulmonary resuscitation," *Jama*, vol. 263, no. 8, pp. 1106–1113, 1990.

[18] G. Bojanov, "Blood pressure, heart tones, and diagnoses," *Handbook of Cardiac Anatomy, Physiology, and Devices*, pp. 181–190, 2005.

[19] B. V. Scheer, A. Perel, and U. J. Pfeiffer, "Clinical review: complications and risk factors of peripheral arterial catheters used for haemodynamic monitoring in anaesthesia and intensive care medicine," *Critical care*, vol. 6, pp. 1–7, 2002.

[20] J. Allen, "Photoplethysmography and its application in clinical physiological measurement," *Physiological measurement*, vol. 28, no. 3, p. R1, 2007.

[21] A. Suzuki and K. Ryu, "Feature selection method for estimating systolic blood pressure using the taguchi method," *IEEE Transactions on Industrial Informatics*, vol. 10, no. 2, pp. 1077–1085, 2013.

[22] Z. Shen, F. Miao, Q. Meng, and Y. Li, "Cuffless and continuous blood pressure estimation based on multiple regression analysis," in *2015 5th international conference on information science and technology (ICIST)*. IEEE, 2015, pp. 117–120.

[23] M. Kachuee, M. M. Kiani, H. Mohammadzade, and M. Shabany, "Cuff-less high-accuracy calibration-free blood pressure estimation using pulse transit time," in *2015 IEEE international symposium on circuits and systems (ISCAS)*. IEEE, 2015, pp. 1006–1009.

[24] F. Miao, N. Fu, Y.-T. Zhang, X.-R. Ding, X. Hong, Q. He, and Y. Li, "A novel continuous blood pressure estimation approach based on data mining techniques," *IEEE journal of biomedical and health informatics*, vol. 21, no. 6, pp. 1730–1740, 2017.

[25] B. Zhang, Z. Wei, J. Ren, Y. Cheng, and Z. Zheng, "An empirical study on predicting blood pressure using classification and regression trees," *IEEE access*, vol. 6, pp. 21 758–21 768, 2018.

[26] E. Mejía-Mejía, J. M. May, M. Elgendi, and P. A. Kyriacou, "Classification of blood pressure in critically ill patients using photoplethysmography and machine learning," *Computer methods and programs in biomedicine*, vol. 208, p. 106222, 2021.

[27] X. Xing and M. Sun, "Optical blood pressure estimation with photoplethysmography and fft-based neural networks," *Biomedical optics express*, vol. 7, no. 8, pp. 3007–3020, 2016.

[28] L. Wang, W. Zhou, Y. Xing, and X. Zhou, "A novel neural network model for blood pressure estimation using photoplethesmography without electrocardiogram," *Journal of healthcare engineering*, vol. 2018, no. 1, p. 7804243, 2018.

[29] M. S. Roy, R. Gupta, and K. D. Sharma, "Bepcon: A photoplethysmography-based quality-aware continuous beat-to-beat blood pressure measurement technique using deep learning," *IEEE Transactions on Instrumentation and Measurement*, vol. 71, pp. 1–9, 2022.

[30] Ü. Şentürk, İ. Yücedağ, and K. Polat, "Repetitive neural network (rnn) based blood pressure estimation using ppg and ecg signals," in *2018 2Nd international symposium on multidisciplinary studies and innovative technologies (ISMSIT)*. Ieee, 2018, pp. 1–4.

[31] P. Su, X.-R. Ding, Y.-T. Zhang, J. Liu, F. Miao, and N. Zhao, "Long-term blood pressure prediction with deep recurrent neural networks," in *2018 IEEE EMBS International conference on biomedical & health informatics (BHI)*. IEEE, 2018, pp. 323–328.

[32] C. El-Hajj and P. A. Kyriacou, "Cuffless blood pressure estimation from ppg signals and its derivatives using deep learning models," *Biomedical Signal Processing and Control*, vol. 70, p. 102984, 2021.

[33] C. Ma, P. Zhang, F. Song, Y. Sun, G. Fan, T. Zhang, Y. Feng, and G. Zhang, "Kd-informer: A cuff-less continuous blood pressure waveform estimation approach based on single photoplethysmography," *IEEE Journal of Biomedical and Health Informatics*, vol. 27, no. 5, pp. 2219–2230, 2022.

[34] U. Senturk, K. Polat, and I. Yucedag, "A novel blood pressure estimation method with the combination of long short term memory neural network and principal component analysis based on ppg signals," in *Artificial Intelligence and Applied Mathematics in Engineering Problems: Proceedings of the International Conference on Artificial Intelligence and Applied Mathematics in Engineering (ICAIAME 2019)*. Springer, 2020, pp. 868–876.

[35] A. Kumar, R. Komaragiri, M. Kumar *et al.*, "A novel cs-net architecture based on the unification of cnn, svm and super-resolution spectrogram to monitor and classify blood pressure using photoplethysmography," *Computer Methods and Programs in Biomedicine*, vol. 240, p. 107716, 2023.

[36] S. Shimazaki, H. Kawanaka, H. Ishikawa, K. Inoue, and K. Oguri, "Cuffless blood pressure estimation from only the waveform of photoplethysmography using cnn," in *2019 41st Annual International Conference of the IEEE Engineering in Medicine and Biology Society (EMBC)*. IEEE, 2019, pp. 5042–5045.

[37] S. S. Mousavi, M. Firouzmand, M. Charmi, M. Hemmati, M. Moghadam, and Y. Ghorbani, "Blood pressure estimation from appropriate and inappropriate ppg signals using a whole-based method," *Biomedical Signal Processing and Control*, vol. 47, pp. 196–206, 2019.

[38] O. Schlesinger, N. Vigderhouse, D. Eytan, and Y. Moshe, "Blood pressure estimation from ppg signals using convolutional neural networks and siamese network," in *ICASSP 2020-2020 IEEE international conference on acoustics, speech and signal processing (ICASSP)*. IEEE, 2020, pp. 1135–1139.

[39] K. R. Vardhan, S. Vedanth, G. Poojah, K. Abhishek, M. N. Kumar, and V. Vijayaraghavan, "Bp-net: Efficient deep learning for continuous arterial blood pressure estimation using photoplethysmogram," in *2021 20th IEEE International Conference on Machine Learning and*

Applications (ICMLA). IEEE, 2021, pp. 1495–1500.

[40] C. Sideris, H. Kalantarian, E. Nemati, and M. Sarrafzadeh, "Building continuous arterial blood pressure prediction models using recurrent networks," in *2016 IEEE International Conference on Smart Computing (SMARTCOMP)*. IEEE, 2016, pp. 1–5.

[41] G. Slapničar, N. Mlakar, and M. Luštrek, "Blood pressure estimation from photoplethysmogram using a spectro-temporal deep neural network," *Sensors*, vol. 19, no. 15, p. 3420, 2019.

[42] J. Esmaelpoor, M. H. Moradi, and A. Kadkhodamohammadi, "A multistage deep neural network model for blood pressure estimation using photoplethysmogram signals," *Computers in Biology and Medicine*, vol. 120, p. 103719, 2020.

[43] S. Baker, W. Xiang, and I. Atkinson, "A hybrid neural network for continuous and non-invasive estimation of blood pressure from raw electrocardiogram and photoplethysmogram waveforms," *Computer Methods and Programs in Biomedicine*, vol. 207, p. 106191, 2021.

[44] M. Gandhi, Y. Pan, E. Theodorou, P. Sebastian, M. Olson, and D. Yannopoulos, "Learning to predict coronary perfusion pressure during cardiopulmonary resuscitation," in *Dynamic Systems and Control Conference*, vol. 51890. American Society of Mechanical Engineers, 2018, p. V001T13A002.

[45] J.-U. Park, D.-W. Kang, U. Erdenebayar, Y.-J. Kim, K.-C. Cha, and K.-J. Lee, "Estimation of arterial blood pressure based on artificial intelligence using single earlobe photoplethysmography during cardiopulmonary resuscitation," *Journal of medical systems*, vol. 44, pp. 1–4, 2020.

[46] L. Jiang, S. Chen, X. Pan, J. Zhang, X. Yin, C. Guo, M. Sun, B. Ding, X. Zhai, K. Li *et al.*, "Estimation of invasive coronary perfusion pressure using electrocardiogram and photoplethysmography in a porcine model of cardiac arrest," *Computer Methods and Programs in Biomedicine*, p. 108284, 2024.

[47] F. Schrumpf, P. Frenzel, C. Aust, G. Osterhoff, and M. Fuchs, "Assessment of deep learning based blood pressure prediction from ppg and rppg signals," in *Proceedings of the IEEE/CVF conference on computer vision and pattern recognition*, 2021, pp. 3820–3830.

[48] X. Xing, Z. Ma, M. Zhang, Y. Zhou, W. Dong, and M. Song, "An unobtrusive and calibration-free blood pressure estimation method using photoplethysmography and biometrics," *Scientific reports*, vol. 9, no. 1, p. 8611, 2019.

[49] G. Martínez, N. Howard, D. Abbott, K. Lim, R. Ward, and M. Elgendi, "Can photoplethysmography replace arterial blood pressure in the assessment of blood pressure?" *Journal of clinical medicine*, vol. 7, no. 10, p. 316, 2018.

[50] J. Park, H. S. Seok, S.-S. Kim, and H. Shin, "Photoplethysmogram analysis and applications: an integrative review," *Frontiers in Physiology*, vol. 12, p. 808451, 2022.

[51] L. Sörnmo and P. Laguna, *Bioelectrical signal processing in cardiac and neurological applications*. Academic press, 2005.

[52] M. Nabian, Y. Yin, J. Wormwood, K. S. Quigley, L. F. Barrett, and S. Ostadabbas, "An open-source feature extraction tool for the analysis of peripheral physiological data," *IEEE journal of translational engineering in health and medicine*, vol. 6, pp. 1–11, 2018.

[53] S. Bengio, O. Vinyals, N. Jaitly, and N. Shazeer, "Scheduled sampling for sequence prediction with recurrent neural networks," *Advances in neural information processing systems*, vol. 28, 2015.

[54] M. Schuster and K. K. Paliwal, "Bidirectional recurrent neural networks," *IEEE transactions on Signal Processing*, vol. 45, no. 11, pp. 2673–2681, 1997.

[55] I. Sutskever, O. Vinyals, and Q. V. Le, "Sequence to sequence learning with neural networks," *Advances in neural information processing systems*, vol. 27, 2014.

[56] D. Bahdanau, "Neural machine translation by jointly learning to align and translate," *arXiv preprint arXiv:1409.0473*, 2014.

[57] A. Vaswani, "Attention is all you need," *Advances in Neural Information Processing Systems*, 2017.

[58] M. Boller, D. J. Fletcher, B. M. Brainard, S. Haskins, K. Hopper, V. M. Nadkarni, P. T. Morley, M. McMichael, R. Nishimura, J. H. Robben *et al.*, "Utstein-style guidelines on uniform reporting of in-hospital cardiopulmonary resuscitation in dogs and cats. a recover statement," *Journal of Veterinary Emergency and Critical Care*, vol. 26, no. 1, pp. 11–34, 2016.